University of Nevada, Reno

Block Kinematics and Slip Rates in the Southern Walker Lane Estimated From GPS Data

A thesis submitted in partial fulfillment of the

requirements for the degree of Master of Science in

Geophysics

by

Sumant Jha

Dr. William C. Hammond/Thesis Advisor

August, 2010

University of Nevada, Reno
Statewide • Worldwide

THE GRADUATE SCHOOL

We recommend that the thesis
prepared under our supervision by

SUMANT JHA

entitled

Block Kinematics And Slip Rates In The Southern Walker Lane Estimated From GPS Data

be accepted in partial fulfillment of the
requirements for the degree of

MASTER OF SCIENCE

William C. Hammond, Ph.D., Advisor

Corne W. Kreemer, Ph.D, Committee Member

Ilia Zaliapin, Ph.D, Graduate School Representative

Marsha H. Read, Ph. D., Associate Dean, Graduate School

August, 2010

Abstract

The southern Walker Lane (SWL) is a part of the Eastern California Shear Zone that lies north of the Mojave region, bounded by the Garlock Fault to the south, the Sierra Nevada to the west, the Basin and Range to the east and by Mono Lake to the north. The region includes many northwest striking right-lateral strike slip and sub-parallel normal faults (e.g. Death Valley/Furnace Creek, Fish Lake Valley, Owens Valley), which together accommodate ~25% of the Pacific/North American relative motion. For many of these faults, and the system as a whole, there appears to be a discrepancy between geodetically and geologically inferred fault slip rates. Since the installation of the EarthScope Plate Boundary Observatory (PBO), and the Nevada Earthquake Response Network (NEARNET) of the University of Nevada, Reno, many recently obtained high-precision GPS data are now available to place improved constraints on the pattern and rates of crustal deformation of this region.

In this study we use a block modeling methodology to estimate block motions and fault slip rates from GPS velocities of PBO, NEARNET and Basin and Range geodetic network (BARGEN) continuous sites. We solve for the motion of blocks using the GPS velocities to estimate long-term motion. In previous geologic studies, fault slip rates have been obtained from the published literature. To evaluate the consistency between the geologic and geodetic data, we compare long-term fault slip obtained from geologic studies to slip rates we infer from the geodetic results obtained over <10 years. We account for transient earthquake cycle effects by incorporating a model of the viscoelastic postseismic relaxation following major historic earthquakes in the region. GPS velocities adjusted for transient effects indicate that there is a distinct NW trend in the motions of the blocks with rates decreasing to the east. The results obtained in this study, suggest that geodetic and geologic fault slip rates in most cases agree with one another to within uncertainties. Some of the faults show lower geodetic rates, which might be due to accommodation of fault slip somewhere in the region, which has not been accounted for in the model.

Acknowledgement

I express my sincere and heartfelt thanks to my thesis advisor, Dr. William C. Hammond, whose guidance and support, from initial to final phases of this work, enabled me to have a better understanding of the topic and the nuances therein. He has supported me throughout my thesis with his patience and knowledge whilst allowing me the room to work in my own way. I attribute the level of my Masters degree to his encouragement and effort and without him this thesis, too, would not have been completed or written. One simply could not wish for a better or friendlier supervisor.

Efforts of Dr. Corné Kreemer, are very much acknowledged in my work. The energy he brings in with the novel ideas, are a boon to each and every project he is involved in. His advice and comments on the research kept the thesis on the right track, and improved my understanding of the various aspects of this work.

I am also thankful to Dr. Ilia Zaliapin for agreeing to be my thesis committee member. The faculty members of Geology department, especially Dr. Steven G. Wesnousky, are heartily thanked for providing the valuable inputs to the research in form of their teachings and courses. Dr. Wesnousky is an outstanding teacher I have ever come across in my academic career. I am indebted to him for providing me with such good guidance during my research work here at UNR.

I am thankful to Bret Pecoraro. He is the first person we look forward to whenever we have to collect GPS data from the field. Without his tireless energy and sincere efforts –

it would have been a herculean task to get all that data needed for this research work. His presence made the work easier for the Nevada Geodetic Laboratory and me.

I extend my sincere thanks to my officemate, Xiaohui Zhou and group mate, Jayne Bormann – they helped me whenever I had some doubts or issues with the project in small but important way.

Another important person to thank will be one of my friends here – Vandana Jha. Being away from your near and dear ones, and the country you loved and lived for a long time is no easy task. Vandana's presence made that easy for me. She gave me solid support and encouragement to finish this thesis in time.

I will be ungrateful, if I do not thank my friend, mentor and guide – in both professional and personal life – Pritam Jha. His knowledge of geology is exemplary and he could present ingenuous solutions to the questions I asked him from thousands of miles away.

A couple of other friends, Ajay Singh and Durgesh, are thanked for their moral support.

Last, I would like to thank God, and my Parent. I cannot thank them enough, but I acknowledge their blessings, wishes and support in whatever I did.

Thank you all.

TABLE OF CONTENTS

Page

LIST OF FIGURES

FIGURE **Page**

LIST OF TABLES

TABLE **Page**

CHAPTER I

INTRODUCTION

The estimation of slip rates will help us predict the strain release rate on faults in the Southern Walker Lane (SWL). Estimation of the fault slip rates is an important aspect for creating a seismic hazard model, as building codes, property insurance premiums etc., depend on them. In this research, I have used Global Positioning System (GPS) data extensively. These data provide the location of a given station at any given point in time. This is necessary because no point on earth is truly stationary, owing to plate tectonic forces that deform the crust. We can measure these motions using GPS data on changes in positions of benchmarks over time. To infer how fast the faults are slipping, I have created a model of the SWL where the crust is comprised of elastic blocks that come into contact at faults. The GPS data constrain relative motion of the blocks, and hence the slip rates on faults.

1.1 Southern Walker Lane

The Southern Walker Lane is located in western Nevada and eastern California States and is an interesting study ground for the kinematics of crustal deformation using GPS velocities. This region is situated to the west of the Basin and Range Province (BRP), and comprises of numerous strike-slip and normal faults which form important component of the Pacific- North America (PANA) plate boundary region. Working together with the

San-Andreas Fault Zone, it accommodates approximately 25% of the 50 mm/yr of relative motion between Pacific and North American plate (Dokka and Travis, 1990, Thatcher et al., 1999, Hammond and Thatcher, 2007).

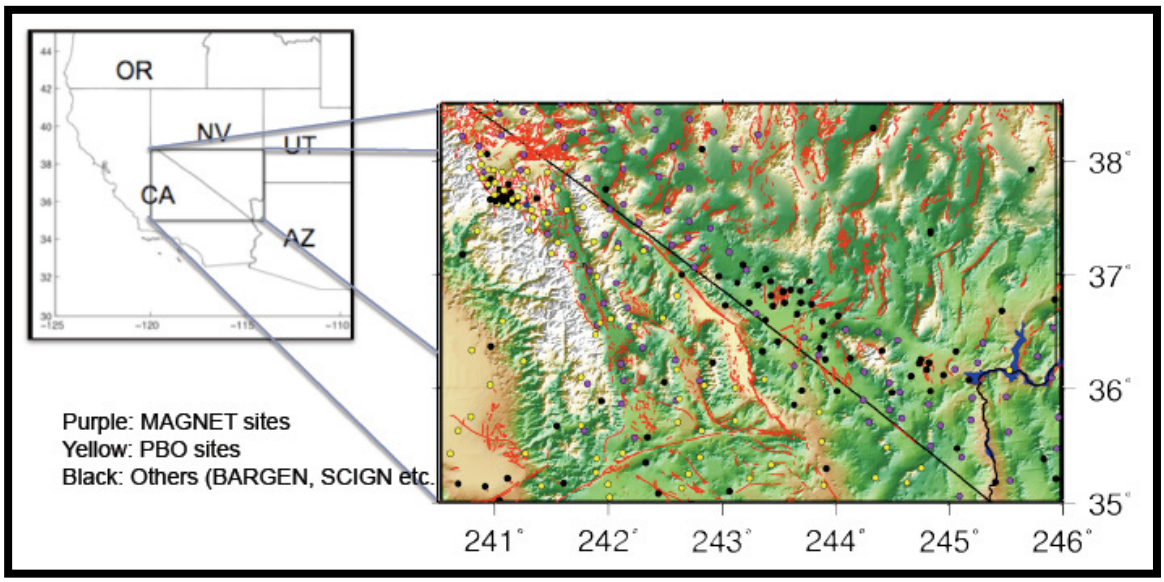

Figure 1: Southern Walker Lane area, lies on the border of CA and NV states. Various permanent, semi-permanent and continuous GPS sites are used to measure the crustal deformation and block motions in the region. The red segments in the figure are Faults and the dots represent the GPS stations (Purple - MAGNET sites, Yellow - PBO sites, Black – Others (BARGEN, SCIGN etc.)

The Southern Walker Lane (Figure 1) extends north of the Mojave region, encompassing the Garlock Fault and extending along the western edge of the Basin and Range. The region includes many northwest striking right-lateral strike-slip faults systems, including the Owens Valley fault and oblique-normal systems like the Panamint Valley – Hunter Mountain – Saline Valley fault systems, and the Death Valley – Furnace Creek – Fish Lake Valley fault systems. The significance of this region is in accommodating both the Basin and Range extension and the PANA transform motion.

1.2 Why study again?

The purpose of this research is to estimate the rates of slip and the motion of blocks and microplates with the help of new GPS data. It has been long known that crustal deformation near fault zones is quantified by long-term slips rates along the faults. In a system of complexly related faults as in Southern Walker lane, the challenge is to quantify the relative importance of each fault, and its contribution to accommodating the total deformation. The San Andreas on the west, is one of the biggest transform fault margins, and is an intriguing feature in itself. This fault along with other faults in the western US are responsible for absorbing the 50 mm/yr motion of the Pacific-North American plates. Out of this 50 mm/yr, ~12 mm/yr is being absorbed by the faults in the southern walker lane. With the availability of many new and recently obtained GPS data, the slip rates along the faults in the SWL warrant a recalculation.

The Basin and Range Province on the east, is a tectonically active feature, which is extending, and resulting in crustal thinning. Kreemer and Hammond (2007) have estimated that the extension in the BRP might be kinematically related to the present shortening in the North California Coast Ranges and Klamath Mountains. Absence of compressional stresses parallel to PA-NA plate boundary permits permanent contraction in the upper plate above southernmost Cascadian subduction zone. The central and northern Walker Lane to the north is an important component in slip transfer from southern walker lane. The purpose of this study is to provide accurate estimates of the slip rates of the faults in the SWL, compare them with the geological estimates along those faults, and present a modified estimate of the slip rate and strain distribution on the

basis of latest geodetic data available to us.

Earlier studies of this nature have calculated the slip rates, which were not consistent with the slip rates obtained by geologic methods (e.g. paleoseismic studies, geochronologic studies etc). For example, Lubetkin, 1988; Beanland and Clarke, 1994 and Lee et. al., 2001b, estimated the fault slip rate for Owen's Valley fault zone, using geological methods as 1-4 mm/yr. The same zone, when measured using GPS data by Reheis and Dixon, 1996; Gan et. al., 2000 and Miller et. al., 2001, yielded various slip rates estimate ranging 2.8 - 7.0 mm/yr. This study, with newest GPS data available to University of Nevada, Reno, the Nevada Bureau of Mines and Geology and the Nevada Geodetic Laboratory - yielded a strike slip rate of 1.1 ± 0.7 mm/yr, across the valley, which agrees better with geologic rates than earlier studies, to within uncertainties.

1.3 Organization of thesis

This thesis is organized in five chapters. The first chapter introduces the area and the need of studying the area again. The second chapter, Data and Methods, presents an overview of how the data are collected, processed and modeled. The third chapter talks about the result obtained from modeling the GPS data, which are then discussed further in fourth chapter, Discussion. The fifth and final chapter presents conclusion and scope of future work in this field.

CHAPTER 2

DATA AND METHODS

The data used in this study were obtained from semi-continuous and continuous GPS networks. The data were collected from the EarthScope Plate Boundary Observatory (PBO), the Mobile Array of GPS for Nevada Transtension (MAGNET), the Nevada Earthquake Response Network (NEARNET), and the Basin and Range Geodetic Network (BARGEN). More than 300 NEARNET sites were surveyed in 2009, providing new station velocities that have improved constraints on the pattern, rate and style of SWL crustal deformation.

2.1 How the data are being collected and processed?

This study is based on collection, processing and interpretation of GPS data. MAGNET is a new kind of GPS network - designed and maintained by Nevada Geodetic Laboratory (Blewitt et al., 2009). This design allows the advantage of better accuracy than tripod surveys and precision close to continuous sites. The semi-permanent or semi-continuous design, allows for a more dense station distribution compared to permanent/continuous GPS networks, owing to lower costs per site and hence, better spatial resolution. This network involves identifying sites, which have unobstructed line of view to sky, and are located on hard bedrocks for each station and installing a GPS pin or mount. The antennas are stationed on these mounts for a part of the year/period, and are circulated among the sites in the network. In this manner, several sites can be covered with a fewer

number of receivers

At each receiver the data are being continuously recorded in compact flash cards at every 15s. These data comprise of station location in north, east and up direction with respect to time. These provide us with the precise location of a given station at any given point in time. After having recorded data for several weeks to several months, data are retrieved and brought back to the laboratory for analysis. These data are converted to RINEX format and then processed using the GIPSY/OASIS II software developed and provided by the Jet Propulsion Laboratory, using Precise Point Positioning system (Zumberge et. al., 1997). Several corrections are applied before the data is converted to station coordinate time series. The reader is referred to Blewitt et. al. (2009) for further details about data processing.

The period of availability of data for each site is summarized in Table 1. These position data are influenced by the transient signals from historical earthquakes in this region.

2.2 Historic earthquakes in the region

In the following paragraphs, we will discuss briefly about the style and magnitude of these earthquakes:

Fort Tejon, 1857: This was one of the biggest earthquakes recorded in the US. As a result of this event, many new cracks formed in the crust, the river courses were changed, and new springs formed. Though the earthquake resulted in the loss of only two lives, it changed the morphology of the region. The earthquake triggered as many as 13 aftershocks, which showed significant correlations between static stress changes and seismicity patterns (Harris and Simpson, 1996). The earthquake produced an offset

ranging from 3 m to 9.5 m along the main 300 km rupture length (Sieh, 1978a). The estimated magnitude was 7.9, based on slip measurements along the faults.

Owens Valley, 1872: This was one of the bigger earthquakes to hit the southern California region, with maximum damage in Lone Pine, where 52 out of 59 houses were destroyed and 27 people were killed in the ensuing aftermath. It resulted in $250,000 destruction of properties [http://www.scec.org]. The earthquake was predominantly strike-slip with a slip of 6 m and rake of 180˚. This is one of the important earthquakes in the region, as the post-seismic response from this more than a century old earthquake are still visible.

Kern County, 1952: This was by far the largest earthquake to have struck the conterminous US, since the 1906 San Francisco earthquake, at that time. The seismic activity in the immediate vicinity of the epicenter of this earthquake was high 1.5 years prior to the main event. Immediately following these sequences, there was a lull of around 2 years. On 21st July 1952 the fault plane became active once more, resulting in $60 million damage to property, and 12 deaths. The magnitude estimated for this earthquake was 7.3. There were 3 noticeable slips of 3.1, 2.6 and 1.1 - all thrust (Stein and Thatcher, 1981)

Chalfant Valley, 1986: The Chalfant Valley earthquake took place in the White Mountain Seismic Gap (Savage and Cockerham, 1987) in Eastern California and resulted in 1.3 and 1.7 m reverse and left lateral slips respectively. The recorded magnitude for this earthquake was M_W 6.2. Though the magnitude is comparatively lesser than the magnitude of other earthquakes used in the correction, the proximity of the event in terms of time and location - forced us to consider its effect. This earthquake took place north of

the Owens Valley earthquake and was located between the Sierra Nevada Range Front, Owens Valley and the White Mountain Fault Zone.

Little Skull Mountain, 1992: On June 29, 1992 – The area of the proposed Yucca Mountain nuclear waste repository experienced a magnitude 5.6 earthquake. This earthquake involved a predominant southeast dip slip motion with small left slip component (Smith et. al., 2001). The main event was followed by 3 major aftershocks - all 4+. The proximity of this earthquake to the proposed nuclear waste site made it an important factor in the design of the site. The earthquake also lies within our study area.

Landers, 1992: One of the largest earthquakes to occur in the United States in last 38 years at that time took place near the town of Landers, CA on June 28, 1992. The recorded magnitude was 7.3. This earthquake resulted in loss of life and properties in the immediate vicinity and broke through 4, then lesser-known, north-south fault lines in the Mojave Desert. On an average, the recorded fault slip was 3-4 m, with a maximum slip of 6 m along these faults.

Hector Mine, October 16,1999: This was the biggest earthquake to have struck in California, since the 1992 Landers earthquake. The remoteness of epicenter from any nearby populated region resulted in no loss, as is normally expected from an earthquake of this magnitude. The earthquake ruptured the north Lavic Lake, central Bullion fault and the south Lavic Lake faults. The earthquake was predominantly strike-slip in nature and resulted in 3 m slip at the maximum. The magnitude was measured at M_w 7.0.

2.3 Post-Seismic correction for collected data

Before the velocity is calculated from position time series, a post-seismic transient is calculated and removed from the GPS time series. The current correction for post-seismic

transient signals, takes into account the Fort Tejon, 1857, Owens Valley, 1872, Kern County, 1952, Chalfant Valley, 1986, Little Skull Mountain, 1992, Landers, 1992, and Hector Mines, 1999 earthquakes. This post-seismic correction uses a Maxwell viscoelastic model to predict how the displacement is dependent on time. The response of the viscoelastic earth following the aforementioned seismic dislocations was modeled using VISCO1D v.3 (Pollitz, 1997). It was assumed that the upper crust is a laterally homogenous, 15-km thick purely elastic layer while the lower crust is also 15 km thick, with Moho being at 30 km depth. The viscosity of the upper mantle and lower crust were assumed to lie in the range of 10^{17} to 10^{21} Pa s. The resulting model prediction was subtracted from the GPS time series before using the data to infer the rate of motion (Hammond et al., 2010).

We observed that the data processed for accounting of the post-seismic relaxation yields slip rate estimates that are in closer agreement to geologic slip rates as compared to the uncorrected data. The logic behind correcting for post-seismic relaxation is that the earthquakes are the result of stress accumulations. In the interseismic stage, the stress is being built up along a fault. The accumulated stress is released in the co-seismic stage, when there is an earthquake. The stress continues to accumulate in the post-seismic stage. Postseismc stress changes can potentially be influenced by after slip, poro-elastic relaxation, viscoelastic relaxation. Recent studies have started accounting for the redistribution of stress owing to post-seismic relaxation.

When modeling post-seismic relaxation, how a model will behave depends on the earthquakes selected. Of the possible postseismic mechanisms we consider only the viscoelastic relaxation in the postseismic phase because this process has been shown to

cause significant motions both far from (>200 km) and long after (>10 years) the earthquakes (Freed et al., 2007; Pollitz et al., 2008). The viscoelastic model for the area is based on the result that the lower crust viscosity 10^{19} Pa s and upper mantle viscosity is between $10^{18.5}$ - 10^{19} Pa S (Hammond et al., 2010). The effect of the correction leads to a change of velocities up to 6 mm/yr for the sites modeled in Hammond et. al., (2010). This is a considerable amount of correction keeping in view that all faults in the SWL have the slip rates in the range of less than 10 mm/yr, and hence an important parameter in the current block modeling.

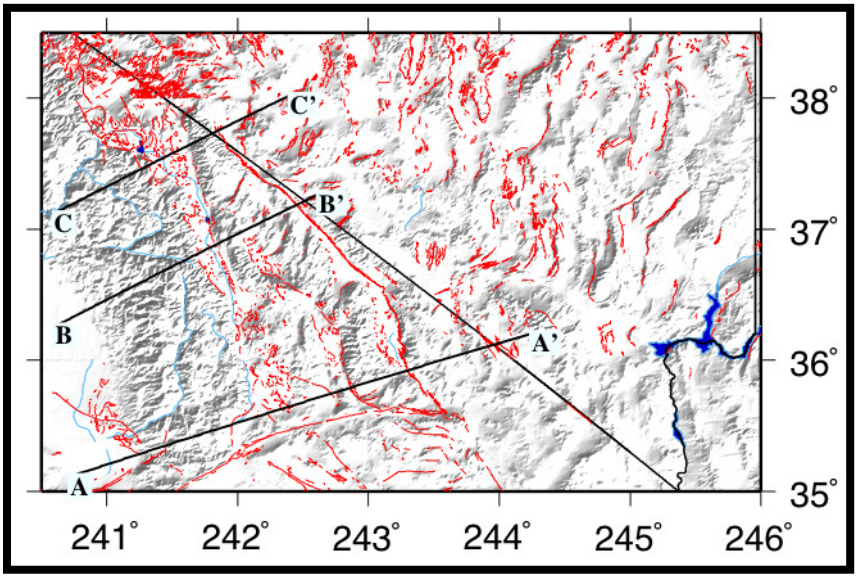

Figure 2. Three sections along AA', BB' and CC' were created in SWL to analyze the size of the signals in the region, and width of zone over which these signal occur etc.

To get an overview of the region, we created three profiles across the SWL, the location of which are shown in Figure 2, and the GPS rates nearest these profiles are shown in Figure 3. What we want to see from these profiles is the size of the signal and the width of the zone over which these signal occurs, whether there are any obvious concentrations of strain rate, and how big are the uncertainties in the region, etc.

2.4 Modeling

After correcting the data for the post-seismic effects of the above-mentioned earthquakes, the time series are modeled in one of two ways. MAGNET sites with time series longer than 2.0 years and less than 3.0 years were modeled with a function that includes linear rate *v*, intercept *b* terms. All other sites were modeled using a function that includes linear rate (v), intercept (b) and annual/semi-annual terms. The uncertainties for these velocities are calculated using the CATS software (Williams, 2003). We assumed that the noise was composed of a combination of white and flicker noise, and the software uses maximum likelihood estimation to estimate the levels of this noise in the series.

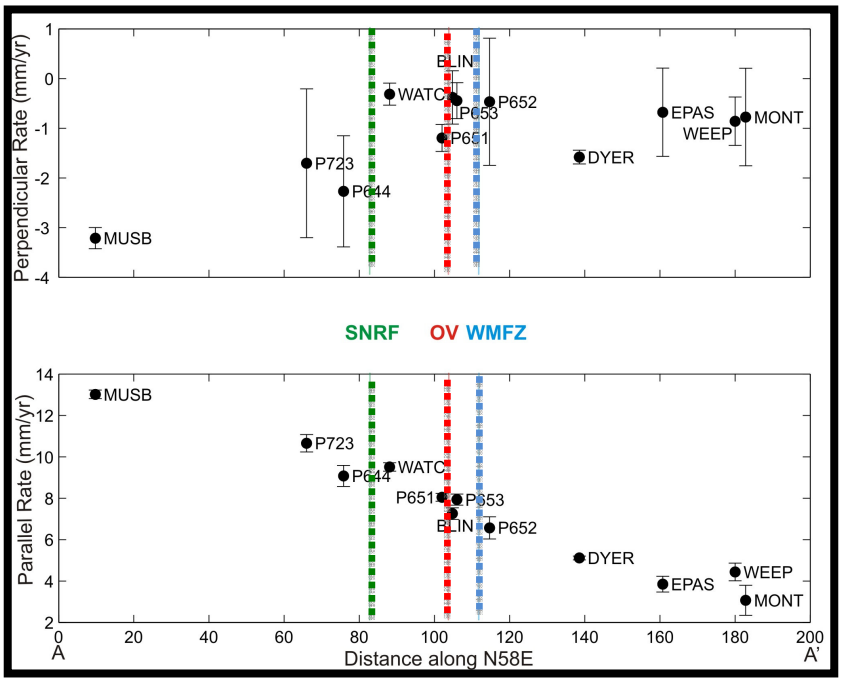

The resulting station velocities and uncertainties (Figure 3) are then used for constraining our block model.

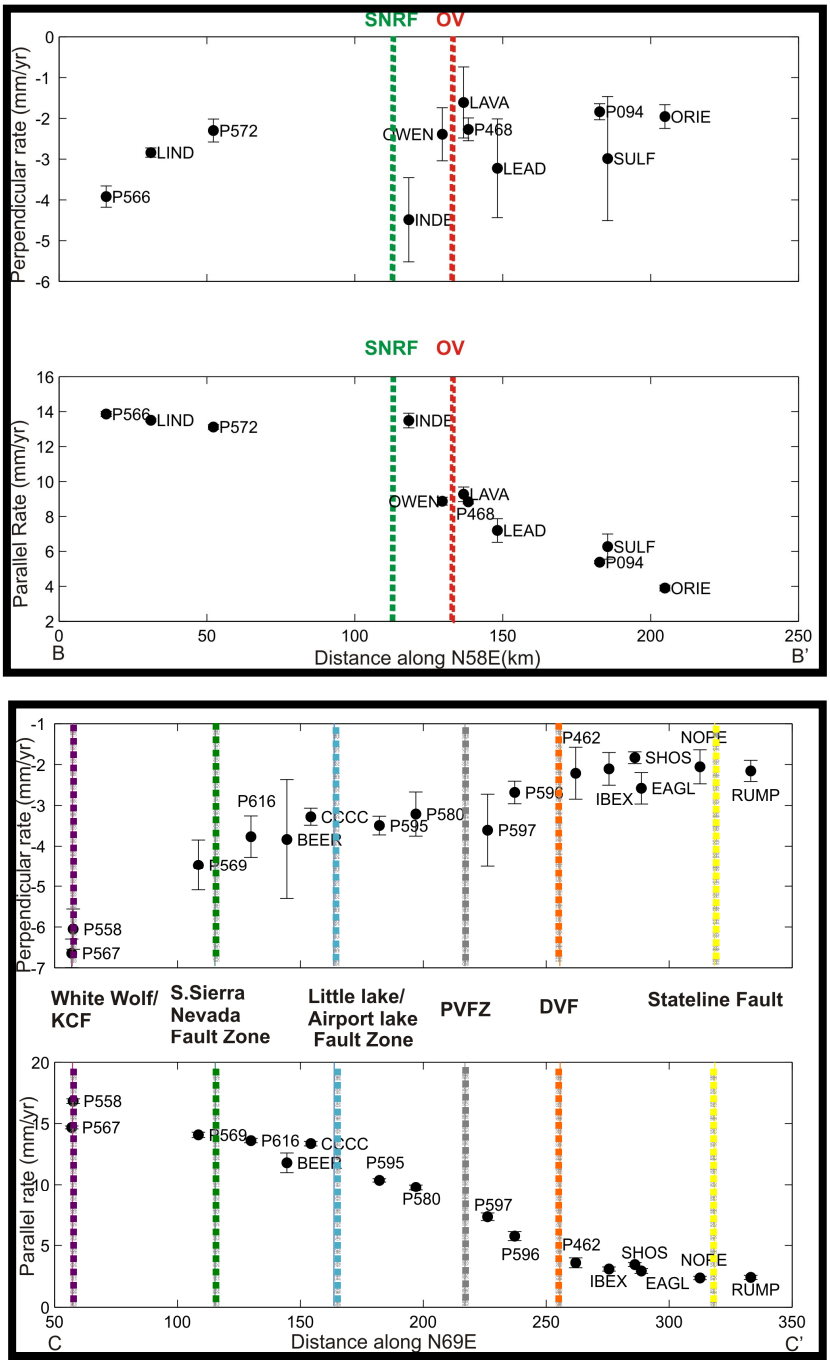

Figure 3: Profile plots across SWL along AA', BB' and CC' (Figure 2) - showing the size of the signal and the width of the zone over which the signal occurs, and uncertainties compared to the signal. The plots are made parallel and perpendicular to the profile lines.

2.4.1 Block Model

Blocks are representations of smaller tectonic entities, which constitute a larger plate. Like large tectonic plates, the motion of these smaller blocks too can be described by rotation about vertical axes, called Euler poles. These poles describe both the rigid block motion (McCaffrey, 2002; Meade and Hager 2005). The bounding faults, which are locked at surface and slipping at depth, create a closed block. Hence, a block is a spherical cap, the motion of which is determined by the ω_x, ω_y, and ω_z vector that is constrained by the GPS velocities on that block. The relative motion across the block boundaries, accounts for interseismic strain which means a) fault slip rate and style are direct consequence of relative block motion, elastic strain accumulation where blocks in contact are locked at surface, and b) slip is continuous along boundaries and changes style with strike (Hammond and Thatcher, 2007).

These blocks (Figure 4) are created using the existing fault and topographic information of the area. In our study, we primarily used the USGS Quaternary Fault and Fold Database, other fault data, and topography. At most of the places, the block boundaries are well constrained by the location of faults. However, at some places, the block boundary has to be inferred on the basis of the topographic features and/or pattern of seismic activities. Another important criterion for placing the block boundaries is the placement of GPS stations. The boundaries are positioned in such a way that there are at least two GPS stations inside each block. This style of boundary selection helps in determining relative velocities of blocks with respect to each other. Once blocks have been defined, each block is identified by a set of nodes, which are described by their latitude and longitude, as shown below:

Node = [latitude, longitude]

Block name = [n_1, n_2, n_3, … , n_n]

The arrangement of the nodes is always in counter-clockwise direction and it is ensured that the numbering of nodes, ensure a closed polygon. For the blocks on the edge of the area of interest, the area boundary is taken as the end of that particular block. Two adjacent nodes that are part of a block boundary identify the surface trace of each fault.

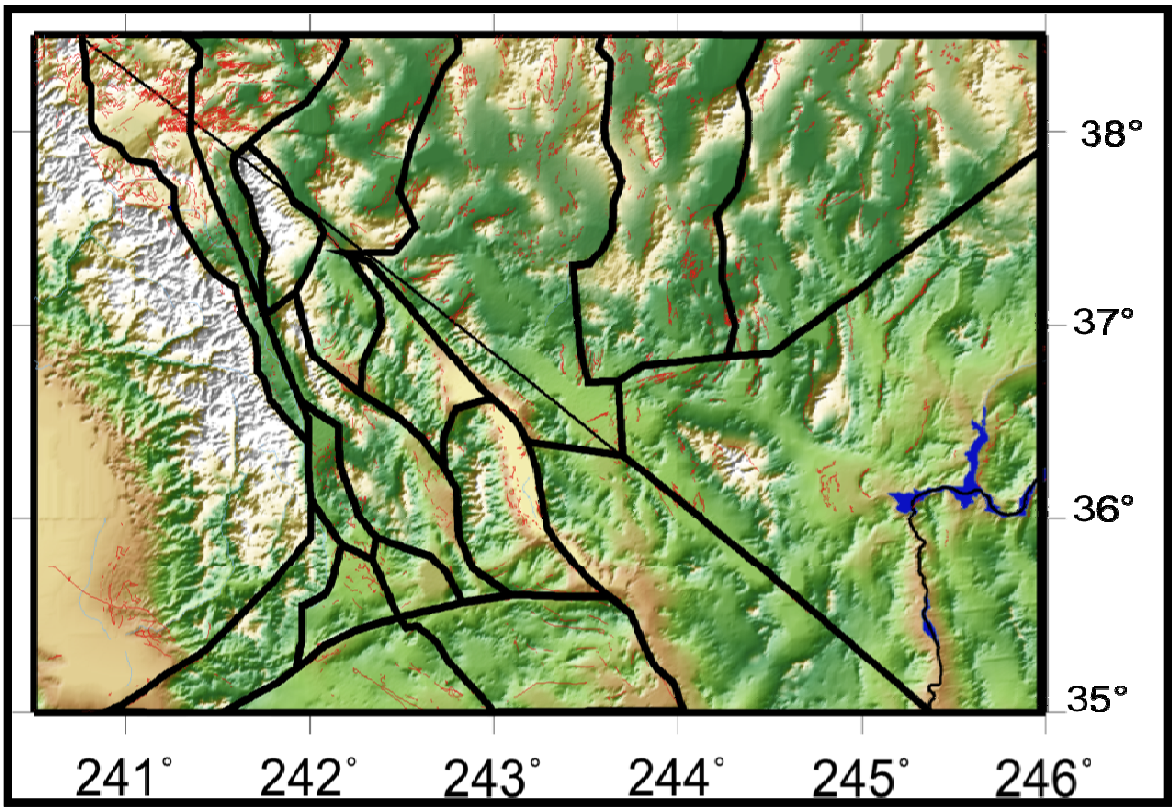

Figure 4: Map showing the Southern Walker Lane divided into different blocks, on the basis of faults and topography in the region.

The faults are denoted in the following notation:

Fault = [from node, to node, locking depth, dip]

The GPS velocities were used to solve for the interseismic velocities across a fault. This interseismic velocity is the residual of the long-term velocity and the coseismic velocity

over several seismic cycles.

This can be represented as -

$$\vec{V}_{Int} = \dot{V}_{LT} - \dot{V}_{Cos}$$

Given the position vector, r_i for GPS velocity vector i on a block j

$$\vec{V}_{GPS,i} = \dot{\omega}_j \times \dot{r}_i - (a_k \dot{G}_{ss,k} + b_k \dot{G}_{N,k})$$

where ωj is unknown block rotation vector, a_k and b_k are unknown slip rotation vectors which scale the greens function G_{ss} and G_N that represents the pattern of strike slip and normal faults for each fault segment denoted by k. G_{ss} and G_N are calculated using Okada functions (1985,1992) since dip, length, and area of the fault are predefined and unit slip is assumed to be sinistral for G_{ss} and updip for G_N. a_k and b_k are determined by the relative motion of the blocks, predefined block geometry and fault dips. The algorithm, also includes the effect on elastic strain accumulation due to multiple nearby fault segment on a given GPS site

$$\vec{v}_{GPS,i} = \dot{\omega} \times \dot{r}_i - \sum_{k=1}^{L} (a_k \dot{G}_{ss,k} + b_k \dot{G}_{N,k})$$

where L is the number of nearest fault segments. Projecting the above velocity in horizontal fields by multiplying the above equation by unit vectors in north and east directions gives us $\vec{v}_{N,i}$ and $\vec{v}_{E,i}$. Ensuring that the relative motion of the blocks is related to the slip rate at the fault, another constraint is used in the following equation

$$\vec{\omega}_{j1} \times \dot{p}_k - \dot{\omega}_{j2} \times \dot{p}_k = a_k \delta\dot{G}_{ss,k} + b_k \delta\dot{G}_{N,k}$$

where $\delta\dot{G}_{ss,k}, \delta\dot{G}_{N,k}$ are full strike-slip and dip-slip motion vector slip rates in the global reference frame across a fault k. The above equations on rearrangement and using vector

equation identities, become

$$v_{N,i} = -\vec{\omega} \bullet (\vec{e}_{N,i} \times \vec{r}_i) - \left[\sum_{k=1}^{L} (a_k \vec{G}_{ss,k} + b_k \vec{G}_{N,k}) \right] \bullet \vec{e}_{N,i}$$

$$\text{and }, v_{E,i} = -\vec{\omega}_j \bullet (\vec{e}_{E,i} \times \vec{r}_i) - \left[\sum_{k=1}^{L} (a_k \vec{G}_{ss,k} + b_k \vec{G}_{N,k} \right] \bullet \vec{e}_{E,i}$$

where $\vec{e}_{N,i}$ and $\vec{e}_{E,i}$ are unit basis vectors at site *i* in the north and east directions respectively. The equation for block rotation vector, ω_j, can be re-written in north and east directions as

$$\vec{\omega}_{J_1} \bullet (-\vec{e}_{N,k} \times \vec{p}_k) + \vec{\omega}_{J_2} \bullet (\vec{e}_{N,k} \times \vec{p}_k) = (a_k \delta \vec{G}_{ss,k} + b_k \vec{G}_{N,k}) \bullet \vec{e}_{N,k}$$

$$\text{and } \vec{\omega}_{J_1} \bullet (-\vec{e}_{E,k} \times \vec{p}_k) + \vec{\omega}_{J_2} \bullet (\vec{e}_{E,k} \times \vec{p}_k) = (a_k \delta \vec{G}_{ss,k} + b_k \vec{G}_{N,k}) \bullet \vec{e}_{E,k}$$

where these equations reproduced from Hammond and Thatcher, (2007).

It has been assumed that normal faults dip at 45 degrees, and strike slip faults at 80 degrees. Also, all locking depth is assumed to be at 15 km depth. A set of apriori values were used to regularize the inversion which are:

1. Slip rate consistency constraints - 0.00001 m/yr
2. Uncertainty in angular rotation - 10^{-8} rad/yr
3. Uncertainty in Slip rates - 0.0003 m/yr
4. Uncertainty in strain rates - 10^{-7}

This study uses a priori uncertainties for rotation vector, slip rates and strain rates, in addition to an apriori constraint for consistency of slip. I tested different sets of apriori values for the angular rotation of each block, slip rates, and strain rates, to analyze the changes on the output.

The equations are solved using the following inputs:

1. Coordinates of the velocity data.
2. Velocity in East and North direction with corresponding uncertainties.
3. Nodes, Blocks and Faults, as described in previous section.

In our study, we have not used the "Up" velocity, Vu, and hence we have assigned "Nan" values to these fields. The calculations also allows to assign apriori values of slip for some of the blocks, which helps us to analyze the effect on remaining blocks, when we try to constrain them using one of the blocks. The outputs, obtained are:

1. List of rotation vectors for each block.
2. Uncertainty in rotation vectors
3. List of slip vectors, one for each fault
4. Uncertainty in slip
5. Strain in each block
6. Uncertainty in strains.

We estimated the effect of changing the fault locking depth to 10 km and 20 km, but found that there was no significant difference in the output. Keeping in accordance with the general agreement about the depth of seismogenic layer in Western United States, it was decided that a fault locking depth of 15 km is an ideal one for SWL.

CHAPTER 3

RESULTS

Using the model created in previous chapter, we estimated the slip rates of each fault and the angular rotation for each blocks in the model, along with their uncertainties. The results are summarized in Table 2 and Table 3. The Block "CB3_4", exhibits maximum angular rotation. This block lies to the south of the Garlock fault and is among the southernmost blocks of the model. We also notice that the Sierra Nevada Great Valley (SNGV) block "SN", is rotating in the opposite sense than the rest of the blocks.

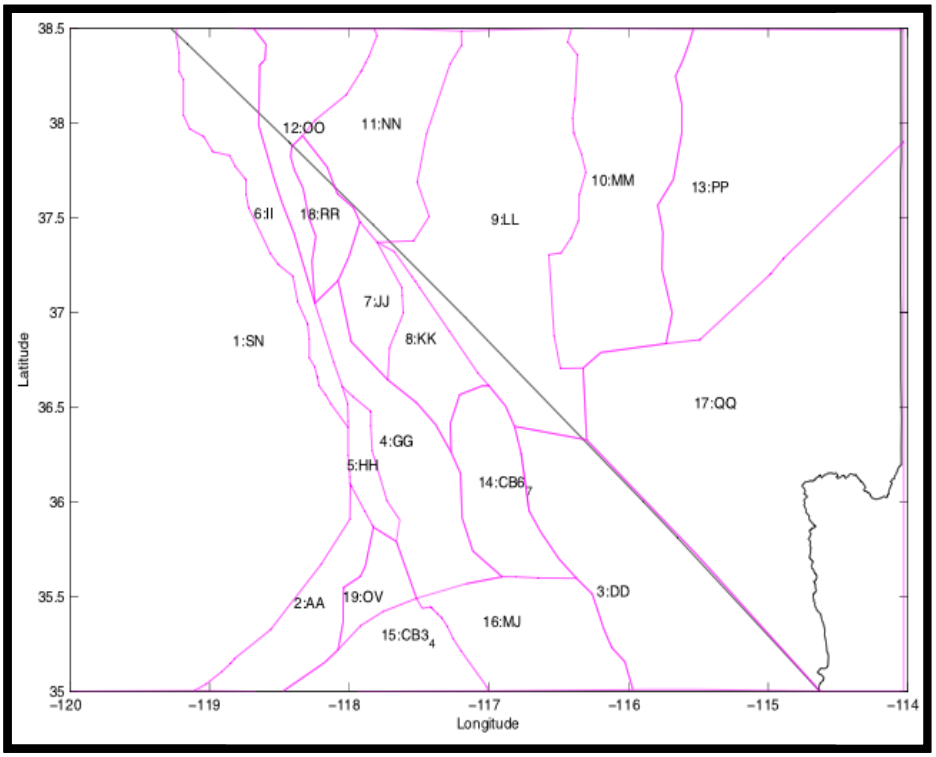

Figure 5. Block diagram showing the names of the blocks

On the basis of the rates obtained after post-seismic correction of data (Figure 3), it seems that there is no obvious concentration of strain in the Owen's Valley region, while there might be some accumulation taking place in the region to the south of Garlock fault. The transform motion of the Pacific plate with the North America plate creates an anti-clockwise rotation effect, which is demonstrated in Figure 6. To constrain the anti-clockwise rotation of the Sierra Nevada (SN) block, we included data from almost the whole SN block, which encompasses an area not totally included in our area of interest. However, it was thought important to include the whole SN, to determine the effect of the rotation in the SWL region.

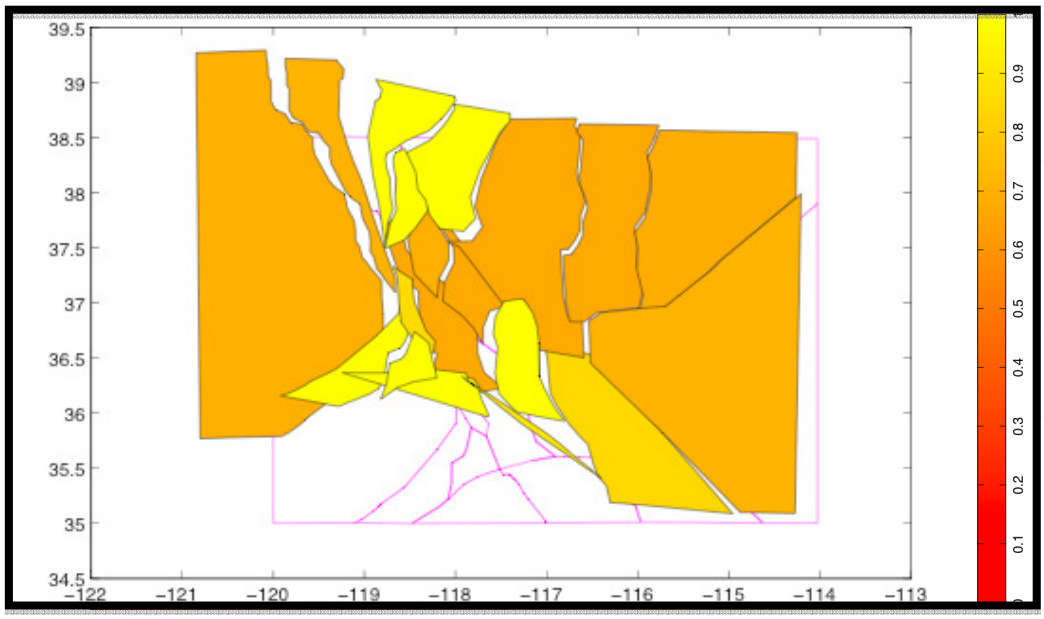

Figure 6. Illustrations of the rotation of SNGV block in anticlockwise direction. Refer Figure 5 for names of blocks shown in this figure. Notice that SNGV block is moving in anti-clockwise direction and away from other blocks in the figure. The color scale represents the rotation color scale factor.

It is also noticed from Table 2, that the strain accumulation is comparably high in "CB3_4", with the maximum strain being in the block "MJ", which is south of the

Garlock fault.

Table 4 shows the slip rates of the faults in the region. These faults, as discussed earlier, are segments along the block boundaries, which together constitute the boundaries of the blocks as well as are representations of the prominent faults in the region. To determine the slip rate along a fault, e.g., Owens Valley Fault, one has to take into account all the fault segments, which constitute the Owens valley fault.

The overall fit of the model to the GPS velocity data is very good (Figure 7). We find that the residuals suggest a good fit between the observed and modeled fault slip rates along the faults. The normalized RMS in north and east direction is 0.9 and

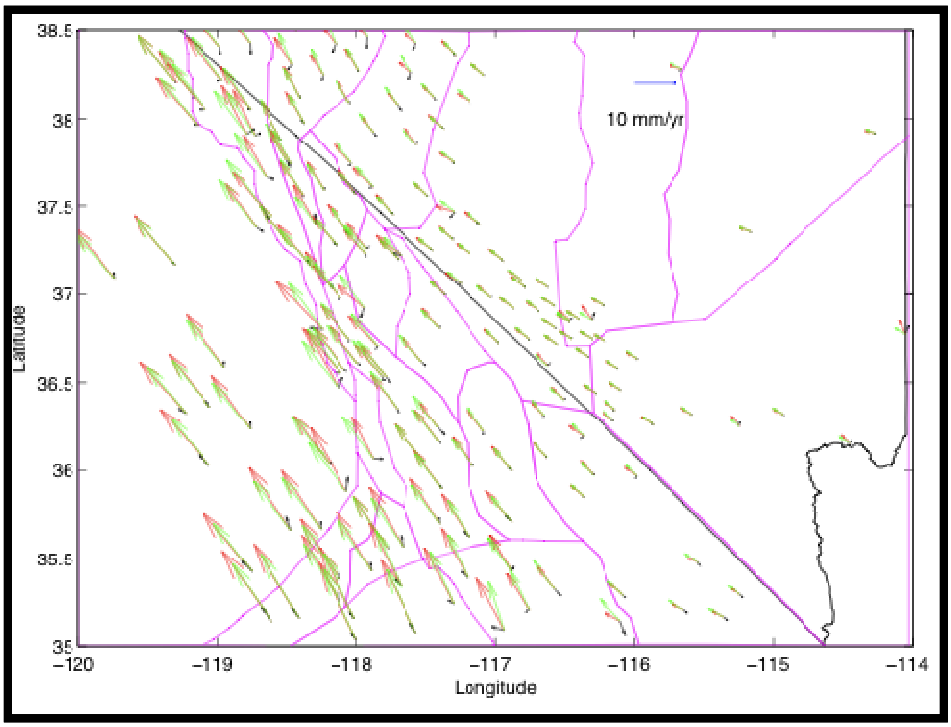

Figure: 7. Overall fit of model velocities (green arrows) with GPS velocities (red arrows). The smaller size of residuals (black arrows) suggests a good fit.

1.0 respectively, which suggest lesser residual variance than our earlier models. We will

discuss the rates and style of deformation of these fault systems in the SWL and the rotation of blocks in the next chapter.

CHAPTER 4

DISCUSSION

We have designed a block model using information about faults and estimated the slip rates along these fault segments and the rotations and strain accumulations associated with the blocks using GPS data as a constraint. It can be seen from figure 8, that the magnitude and pattern of fault is changing along different faults. In this section, we will discuss the implications of these changes of style and magnitude of fault slip rates along some of the faults.

We will start by discussing the various fault systems in the region, the previous studies along those faults and how our results compare with earlier results.

4.1 Owens valley fault zone

Owens Valley is located along the northern part of the Eastern California shear zone, and is characterized as a zone of right lateral shear and extension accommodated Owens Valley Fault Zone, and a series of connecting normal faults such as Towne pass - Emigrant, Tin Mountain, and Deep Springs Faults (Figure 9). We have two profiles crossing the Owens Valley (Profile AA' and Profile BB'). As is seen in Profile BB', the rates parallel to the profile are changing from west to east, with rates being ~12-14 mm/yr for west of OV, and ~4-8 mm/yr to the east. The strike of the fault, it seems, is also playing some role, in the estimation of fault slip rates. The strike of the faults across the

region is changing from 142° to 157°. It is noticed that the slip of the faults are all right lateral strike slip.

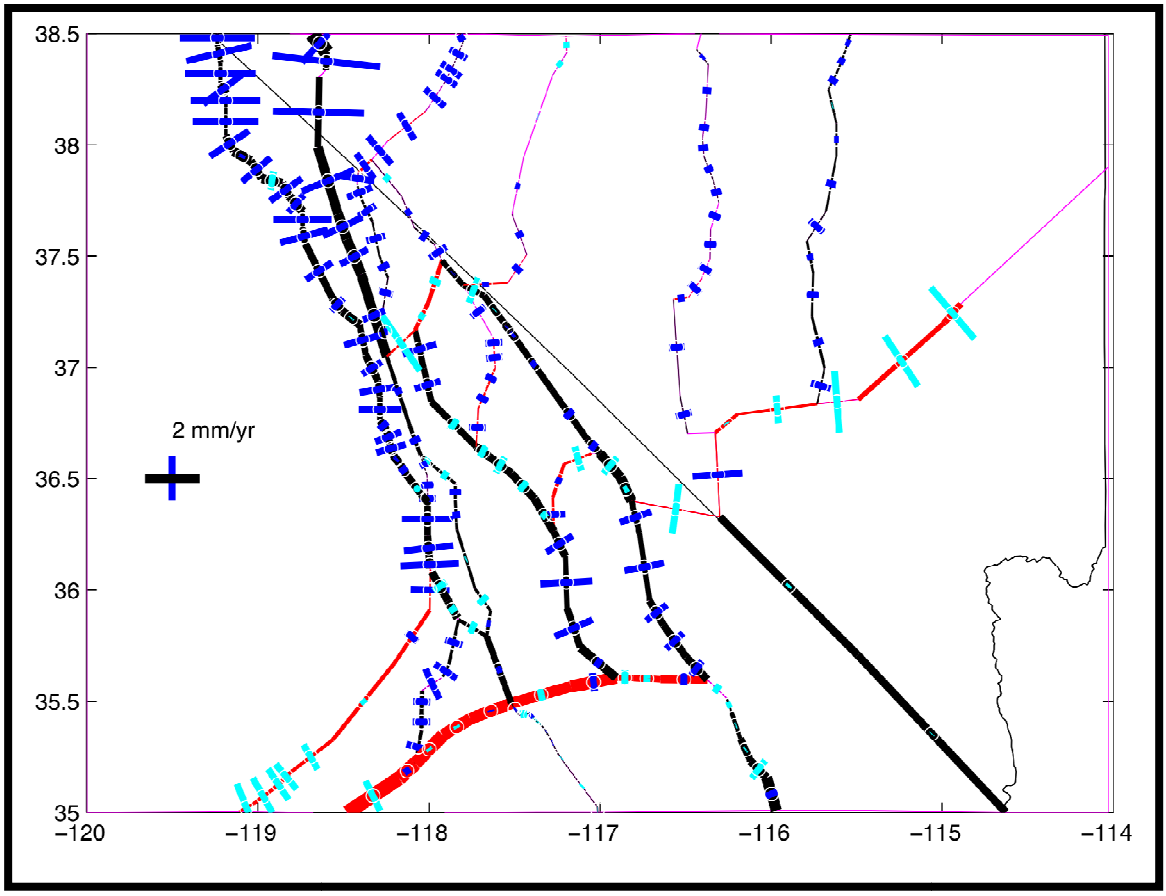

Figure 8. Southern Walker Lane strike slip and extension/thrust slip rates.

The rates of slip are changing from Sierra Nevada Range Front fault in west to Death Valley fault in east, owing to the change in pattern of faulting in the region. The strike slip rate for SNRF is 1.02 ± 0.89 and that for Death Valley fault is 1.39 ± 0.49.

Our slip rates estimate for the Owens Valley fault zone stand at 1.1 ± 0.7 mm/yr which are in agreement with the geologic slip rates in the region. Earlier studies of similar nature have yielded the geodetic slip rates of the region in the range of 4.0 - 8.5

mm/yr (Dixon et. al., 2000; Gan et. al., 2000), which are 4-8 times the geodetic slip rates estimated in this research. The difference between the earlier geodetic and current studies arises because of the greater number of blocks modeled in the region and accounting for viscoelastic properties of lower crust and upper mantle.

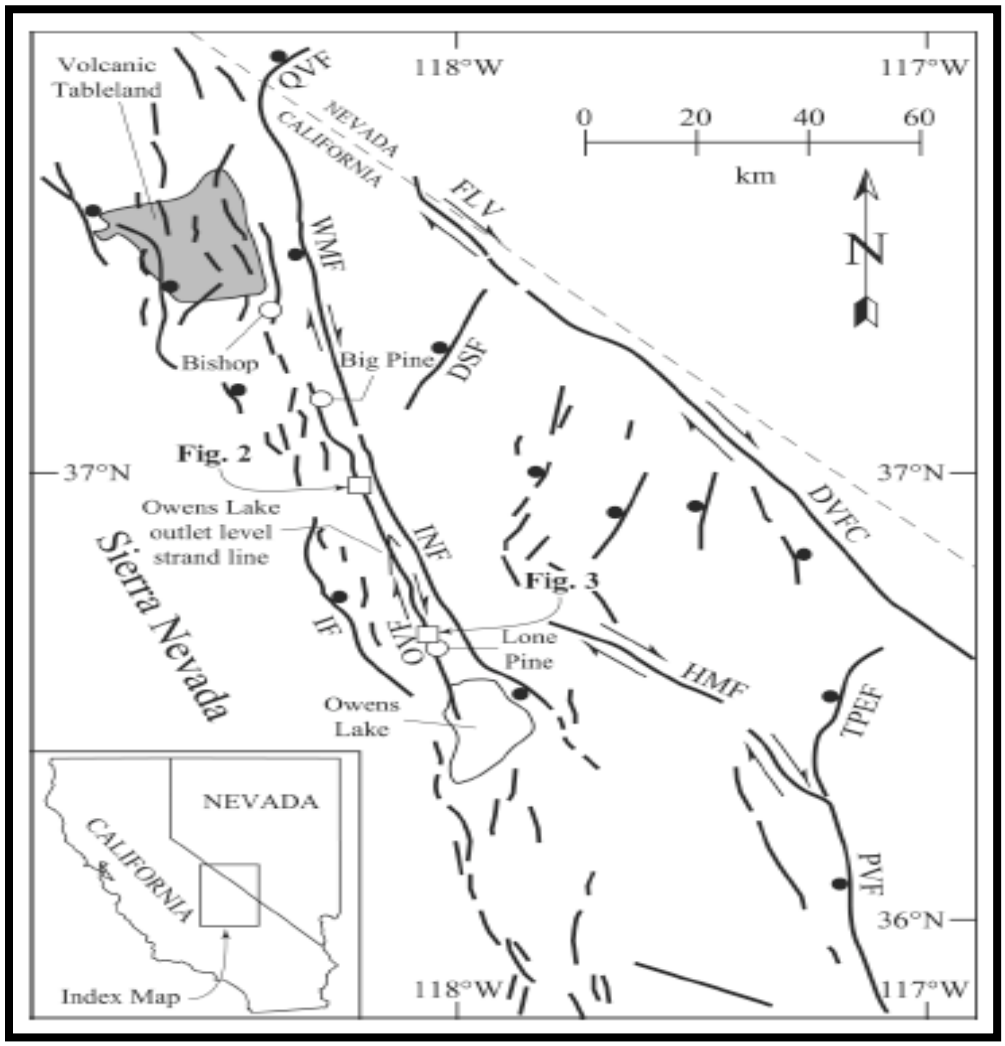

Figure 9. Index map of major Quaternary faults in northern part of Eastern California Shear Zone. DSF—Deep Springs fault, DVFC—Death Valley–Furnace Creek fault zone, FLV—Fish Lake Valley fault zone, HMF—Hunter Mountain fault, IF—Independence fault, INF—Inyo Mountains fault zone, OVF—Owens Valley fault, PVF—Panamint Valley fault, QVF—Queen Valley fault, TPEF—Towne Pass–Emigrant fault system, WMF—White Mountains fault. Solid circle is on hanging wall of normal faults, and arrows indicate relative motion across strike-slip faults (source: Lee et. al., 2001)

4.2 White mountain fault zone

Between 37° and 38° latitude, Owens Valley - White Mountain Fault System, and Death Valley - Fish Lake Valley Fault system and Sierra Nevada Range Front, account for accommodating the most of the 25% North America - Pacific Plate relative motion. Earlier studies on White Mountain fault zone, suggested a geodetic slip rate in the range of 2.2 - 4.6 mm/yr (Reheis and Dixon, 1996) which are very different from that obtained geologically. Kirby et. al., 2006 (Figure 9) studied a sequence of exposed alluvial deposits, and determined the fault slip rate for Late Pleistocene to present using ^{36}Cl dating of alluvial fan surfaces. Their results suggest a value of 0.35 ± 0.5 m/kyr rate for the WMFZ. We have considered WMFZ, as shown in Figure 10. The strike of this fault, as per our model, is varying from 227 to 176 and the slip rate is varying from 0.8 to 0.2 mm/yr. These small segments together make up the entire fault, and give us a very good idea of how the slip rate is varying along the strike. In this case the slip rate is increasing on the WMFZ from SE to NW. To estimate the normal slip rate across the full fault segment, we have averaged the slip rates of the small constituent segments, which yield an estimate of 0.3 ± 0.2 mm/yr, which is in very good agreement with what has been obtained by geologic methods.

4.3 White wolf fault

The White Wolf fault lies in the southwest part of our research area, and has one of the most difficult fault slip rate to estimate. The reason for this is that we have very few geodetic data available from this region. There are only two GPS stations, which provide good constraints for estimating slip rate. The white wolf section, is

geographically close to the Kern County Canyon fault – which is another important fault in this region,

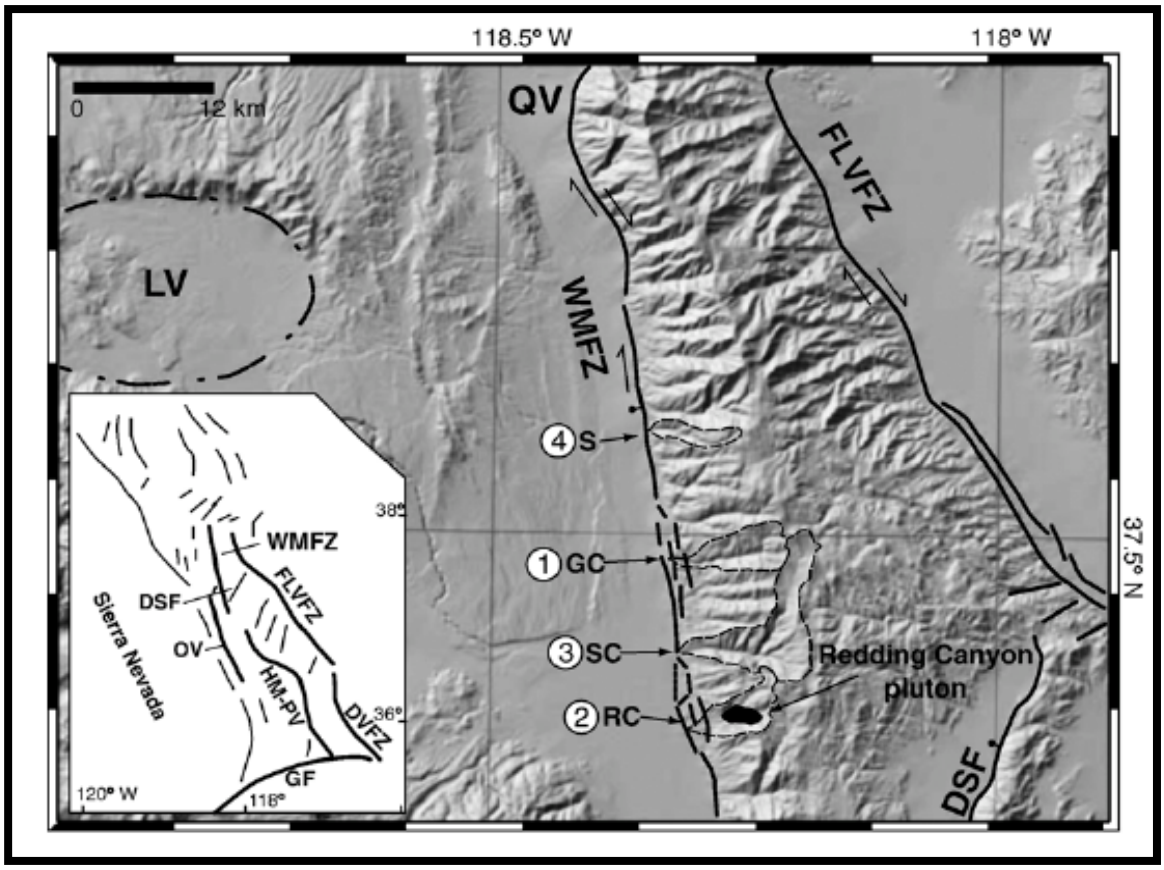

Figure 10: Tectonic setting of the White Mountain Fault Zone (WMFZ). Abbreviations as follows: DSF—Deep Springs fault, DVFZ—Death Valley fault zone, FLVFZ—Fish Lake Valley fault zone, GF—Garlock fault, HM-PV—Hunter Mountain/Panamint Valley fault zone, LV—Long Valley caldera, OV—Owens Valley fault, QV—Queen Valley. Slip rate sites referred to in text: 1—Gunter Creek, 2—Redding Canyon, 3—Silver Canyon, and 4— Sabies Creek. Watersheds are shown as dashed lines. (Source: Kirby et. al., 2006)

which has been referred to as "an important fault within southern Sierra Nevada, whose scarp is one of the few known cases of true fault line scarps" (Webb, 1936). Since then, the fault has not received much of an attention till the 1952 Kern County earthquake, the

details of which are given in earlier sections. There have been a few recent studies on the Kern Canyon fault, notably by Saleeby et. al. 2009 and Nadin and Saleeby, 2008, suggest that the Kern County Fault and its southern extension - the white wolf fault, have been displaced up to ~10 ± 5 km reverse displacement on the eastern side and ~25 km of normal shortening on the southern end, across a period ranging from 95 Ma - 80 Ma.

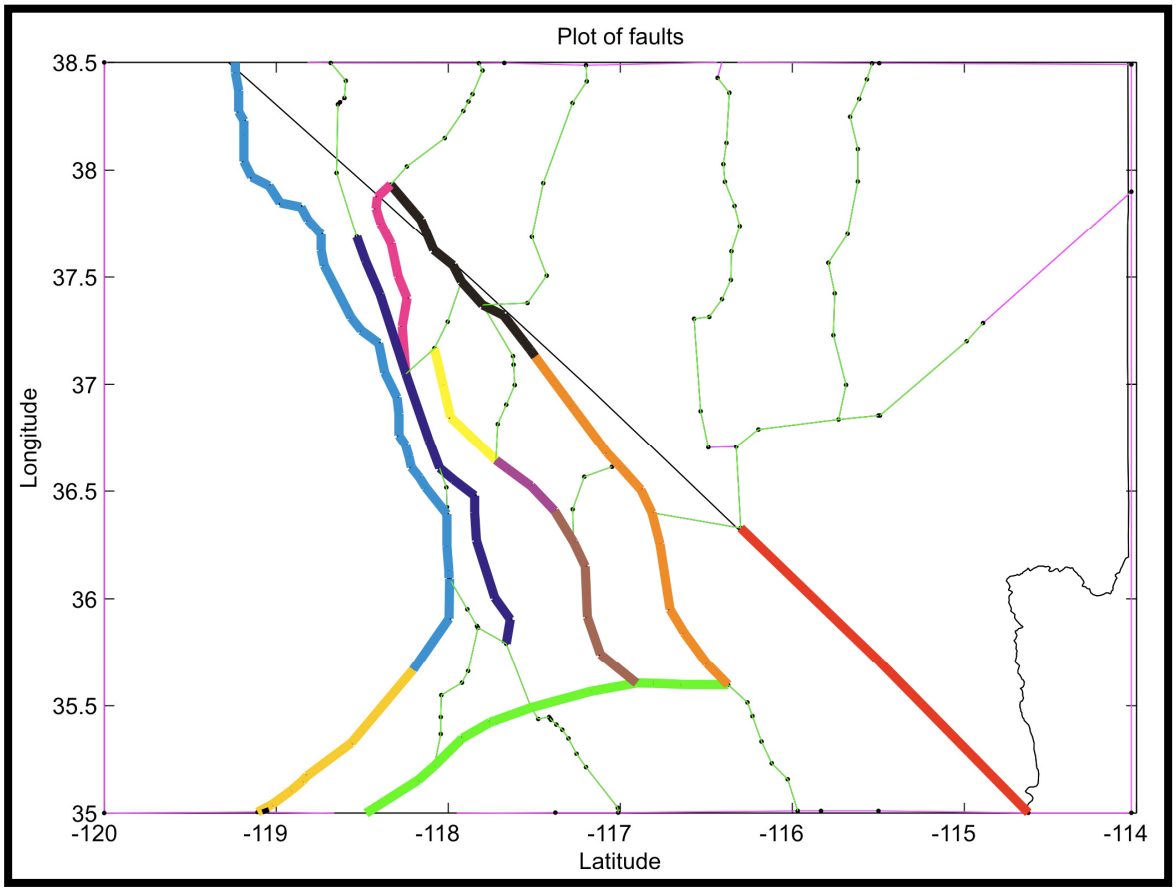

Figure 11: Faults used in model shown in different color. (Red: Stateline Fault, Blue: Sierra Nevada Range Front, Green: Garlock Fault, Purple: Owens Valley Fault, Pink: White Mountain Fault Zone, Black: Fish Lake Valley Fault Zone, Yellow: Hunter Mountain Fault Zone, Brown: Panamint Valley Fault Zone, Orange: Death Valley Fault Zone, Gold: White Wolf Fault)

Kelson et. al., 2009, estimated the fault slip rate for the KCF as 0.3 mm/yr. using geologic and seismologic methods.

Our estimate for the White Wolf section results in a slip rate of 0.4 ± 0.2 mm/yr, on the basis of only a few GPS velocities obtained in this region.

The faults used in this study are shown in figure 11. The locations of these faults are approximated on the basis of the information obtained from USGS quaternary fault fold database, as well as previous literature for e.g. Lee et. al., 2001; Kirby et. al., 2006 etc. These faults are made of smaller fault segments (Figure 11b). Taking the mean of the slip rate along these smaller fault segments derives the slip rate along a fault.

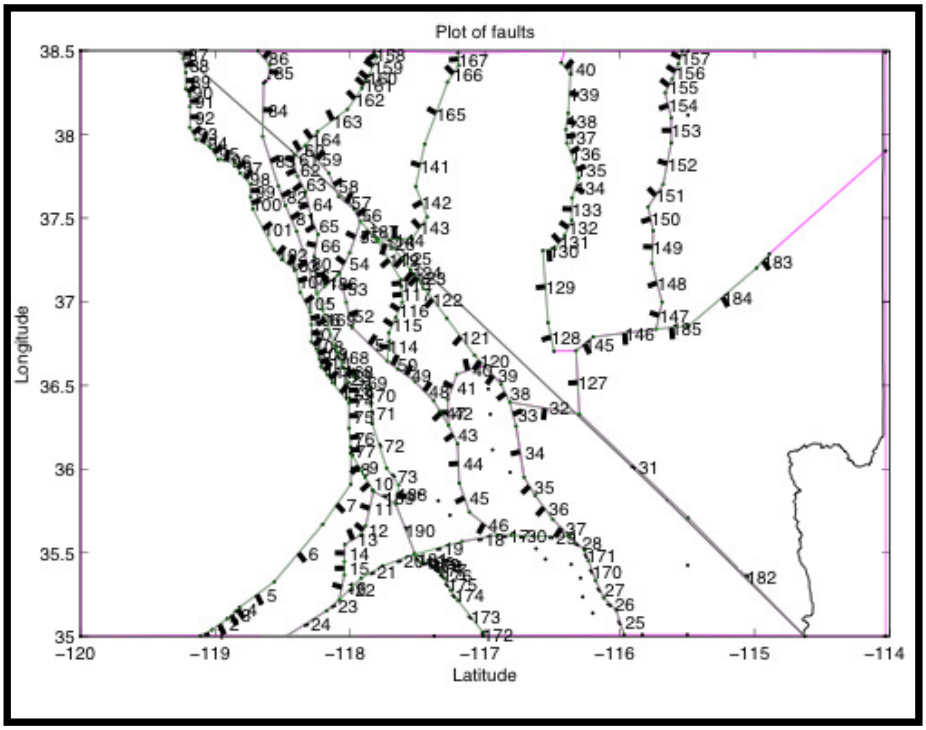

Figure 11b: Block diagram of the region, showing smaller fault segments that comprise bigger fault segments in figure 11.

CHAPTER 5

CONCLUSION

This study focused on estimating SWL fault slip rates using the GPS data. The goal was to estimate the fault slip rates using the new GPS data to come up with best possible rates taking into account the processes like viscoelastic relaxation into account in the region and compare these rates to the geologically estimated slip rates along the faults. The results suggest that the fault slip rates along all the faults are comparable to geologic slip rates except the Hunter Mountain Fault Zone, and the Death Valley Fault Zone (Figure 12). These two have higher geologic slip rates compared to our results as against all previous such studies on these faults where the geodetic slip rates were higher. Considering that the earlier GPS fault slip rate estimates, were either higher than the geologic rates (Gan et. al., 2000) or were in conformation with geologic rates (this study), low fault slip rate estimate of HMFZ, and DVFZ is puzzling., The possible reasons for this disagreement can be due to the fact that we have not allowed the blocks in our model to deform. Or alternatively, that fault slip rates are changing over geologic time i.e. that the fault slip rates being measured with GPS are in the higher slip rate cycle. Another possibility is that fault slip rates are higher for these two faults because the viscoelastic model is somehow not correct and that the uncertainty for the fault slip rates are greater than what we have calculated. It is also possible that our model is more detailed than any other previous model, and accounts for more faults in the region, which distributes the

slip rates among a greater number faults, thereby estimating slip rates that are lower than in other geodetic studies.

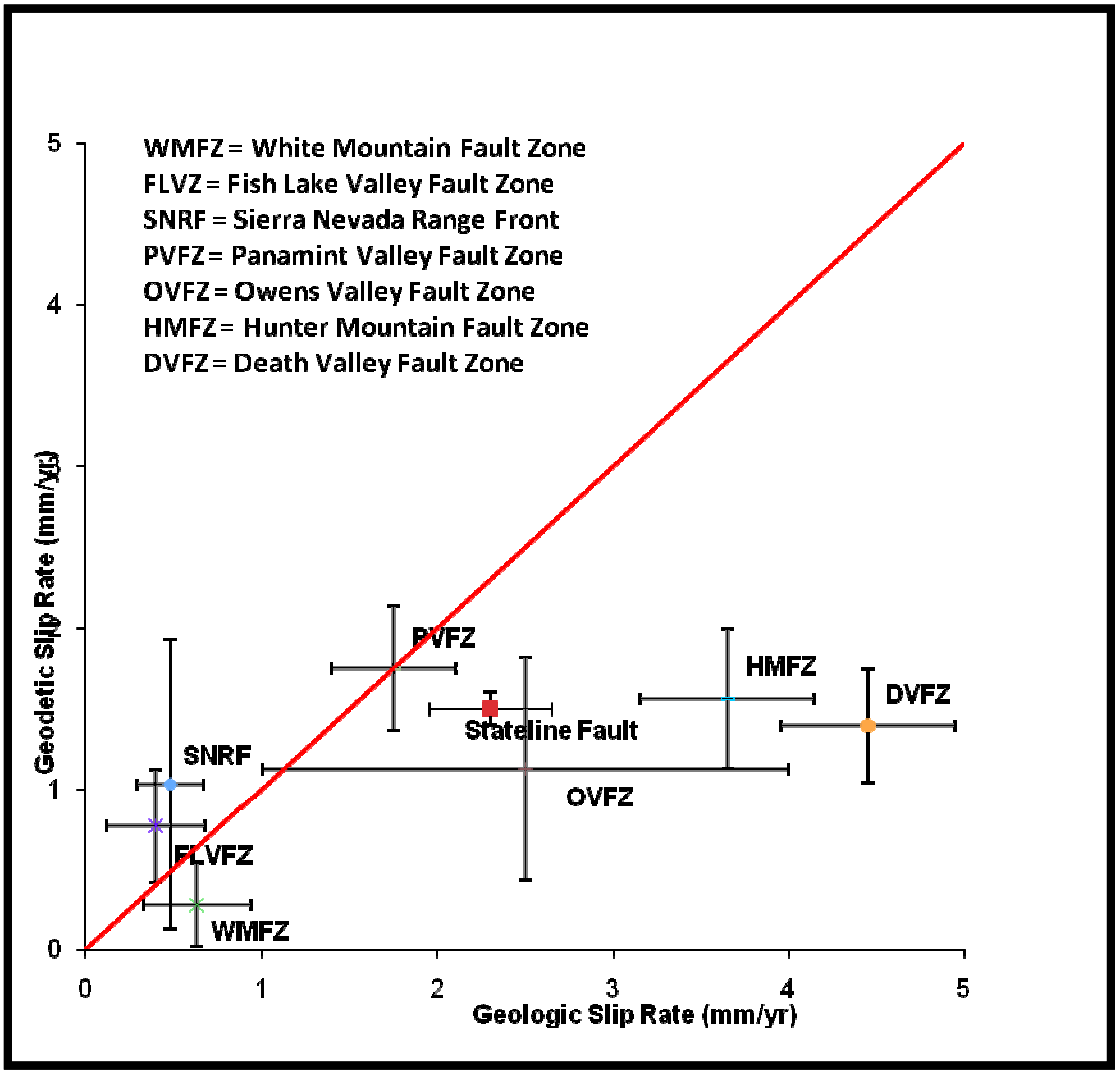

Figure 12: Comparison between geologic and geodetic fault slip rates. Error bars represent 2-sigma uncertainty in slip rate.

REFERENCES

Beanland, S., and M. M. Clark (1994), The Owens Valley fault zone, eastern California, and surface rupture associated with the 1872 earthquake, U.S. Geological Survey Bulletin, 1982, 1-29.

Bendick, R., Bilham, R., Fremuller, J., Larson, K. and Yin, G. (2000), Geodetic evidence for a low slip rate in the Altyn Tagh fault system, Nature, vol. 404, 69-72

Blewitt, G., C. Kreemer, and W.C. Hammond (2009). Geodetic observation of contemporary deformation in the northern Walker Lane: 1. Semipermanent GPS strategy, p. 1–15, doi: 10.1130/2009.2447(03).

dePolo, C. M. (1989), Seismotectonics of the White Mountains fault system, east-central California and west-central Nevada, Master's thesis, Mackay Sch. of Mines, Univ. of Nev. Reno, Reno.

Dixon, T. H., et al. (2000), Present-day motion of the Sierra Nevada block and some tectonic implications for the Basin and Range province, North American Cordillera, Tectonics, 19, 1-24.

Dziewonski, A. M., and D. L. Anderson (1981), Preliminary reference Earth model, Physics of the Earth and Planetary Interiors, 25, 4, 297-356.

Fialko, Y., M. Simons, and D. Agnew (2001), The complete (3-D) surface displacement field in the epicentral area of the 1999 M(w)7.1 Hector Mine earthquake, California, from space geodetic observations, Geophysical Research Letters, 28, 16, 3063-3066.

Frankel, ., et al. (2007), Cosmogenic 10Be and 36Cl geochronology of offset alluvial fans along the northern Death Valley fault zone: Implications for transient strain in the eastern California shear zone, J. Geophys. Res., 112, B06407, doi:10.1029/2006JB004350.

Frankel et. al., (2007) Spatial Variation in slip rate along the Death Valley-Fish lake Valley fault system determined from LiDar topographic data and cosmogenic 10Be geochronology, Geophysical Research Letters, vol. 34, L18303, Doi:10.1029/2007GL030549.

Gan, W. J., J. L. Svarc, J. C. Savage, and W. H. Prescott (2000), Strain accumulation across the Eastern California Shear Zone at latitude 36_300N, J. Geophys. Res., 105, 16,229 – 16,236.

Hammond, W. C., C. Kreemer, and G. Blewitt (2009), Geodetic constraints on contemporary deformation in the northern Walker Lane: 3, Postseismic relaxation in the Central Nevada Seismic Belt, Late Cenozoic Structure and Evolution of the Great Basin –

Sierra Nevada Transition, in press.

Hammond, W. C., and W. Thatcher (2004), Contemporary tectonic deformation of the Basin and Range province, western United States: 10 years of observation with the Global Positioning System, J. Geophys. Res., 109, B08403, doi:10.1029/2003JB002746.

Hammond, W. C., and W. Thatcher (2007), Crustal deformation across the Sierra Nevada, northern Walker Lane, Basin and Range transition, western United States measured with GPS, 2000–2004, J. Geophys. Res., 112, B05411, doi:10.1029/2006JB004625.

Kelson, K., Kozaci, O., Lutz, A., Turner, R., Amos, C., Baldwin, J., Unruh, Brossy, C., Simpson, D., Kozlowicz, B., Rose, R., (2009), Recent Advancements In Understanding Seismic Source Characteristics Of The Kern Canyon Fault, Southern Sierra Nevada, AEG Annual Meeting-2009, Abstracts.

Kirby, E., D. W. Burbank, M. Reheis, and F. Phillips (2006), Temporal variations in slip rate of the White Mountain Fault Zone, Eastern California, Earth and Planetary Science Letters, 248, 1-2, 168-185.

Klinger, R. E. (2001), Evidence for large dextral offset near Red Wall Canyon, in Quaternary and Late Pliocene Geology of the Death Valley Region: Recent Observations on Tectonics, Stratigraphy, and Lake Cycles, edited by M. N. Machette, M. L. Johnson, and J. Slate, U.S. Geol. Surv. Open File Rep., 01-51, A32– A37.
Kreemer C., G. Blewitt, and W.C. Hammond (2009). Geodetic constraints on contemporary deformation in the northern Walker Lane: 2. Velocity and strain rate tensor analysis, p. 17–31, doi: 10.1130/2009.2447(03).

Lee, J., J. Spencer, and L. Owen (2001b), Holocene slip rates along the Owens Valley Fault, California; Implications for the recent evolution of the Eastern California Shear Zone, Geology, 29, 819 – 822.

Lubetkin, L. K. C. (1988), Late Quaternary activity along the Lone Pine Fault, eastern California, Geol. Soc. Am. Bull., 100, 755 – 766.

M Meghan Miller, Daniel J. Johnson, Timothy H Dixon, and Roy K. Dokka, 2001, Refined kinematics of the Eastern California shear zone from GPS observations, 1993-1998. Journal of Geophysical Research. v. 106, p. 2245-2264.

McClusky, S. C., et al. (2001), Present day kinematics of the Eastern California Shear Zone from a geodetically constrained block model, Geophys. Res. Lett., 28, 3369-3372.

Murray, M. H., J. C. Savage, M. Lisowski, and W. K. Gross (1993), Coseismic Displacements - 1992 Landers, California, Earthquake, Geophysical Research Letters, 20, 7, 623-626.

Nadin, E.S., and Saleeby, J.B., 2008, Disruption of regional primary structure of the Sierra Nevada batholith by the Kern Canyon fault system, California, in Wright,J.E., and Shervais, J.W., eds., Ophiolites, Arcs, and Batholiths: Geological Society of America Special Paper 438, doi: 10.1130/2008.2438(15).

Oswald, J. O., and S. G. Wesnousky (2002), Neotectonics and Quaternary geology of the Hunter Mountain fault zone and Saline Valley region, southeastern California, Geomorphology, 42, 255 – 278.

Pancha, A., J. G. Anderson, and C. Kreemer (2006), Comparison of seismic and geodetic scalar moment rates across the Basin and Range province, Bulletin of the Seismological Society of America, 96, 1, 11-32, doi:10.1785/0120040166.

Pollitz, F. F. (1997), Gravitational-viscoelastic postseismic relaxation on a layered spherical Earth, Journal of Geophysical Research, 102, 17,921-917,941.

Reheis, M. C., and T. H. Dixon (1996), Kinematics of the Eastern California Shear Zone: Evidence for slip transfer from Owens and Saline Valley fault zones to Fish Lake Valley fault zone, Geology, 24, 339 – 342.

Reheis, M. C., and T. L. Sawyer (1997), Late Cenozoic history and slip rates of the Fish Lake Valley, Emigrant Peak, and Deep Springs fault zone, Nevada and California, Geol. Soc. Am. Bull., 109, 280–299

Saleeby, J., Saleeby, Z., Nadin, E. and Maheo, G.(2009) 'Step-over in the structure controlling the regional west tilt of the Sierra Nevada microplate: eastern escarpment system to Kern Canyon system', International Geology Review, 51: 7, 634 — 669

Shen, Z. K., et al. (2003), The SCEC Crustal Motion Map, Version 3.0.

Smith, K. D., J. N. Brune, D. M. dePolo, M. K. Savage, R. Anooshehpoor, and A. F. Sheehan (2000), The 1992 Little Skull Mountain Earthquake Sequence, Southern Nevada test Site, in Geologic and Geophysical Characterization studies of Yucca Mountain, Nevada, A potential high-level radioactive waste repository, edited by J. W. Whitney and W. R. Keefer, U.S. Geological Survey, U.S. Department of the Interior.

Stein, R. S., and W. Thatcher (1981), Seismic and aseismic deformation associated with the 1952 Kern County, California, earthquake and relationship to the Quaternary history of the White Wolf Fault, Journal of Geophysical Research, 86, B6, 4913-4928.

Wdowinski, S., Y. Bock, J. Zhang, P. Fang, and J. Genrich (1997), Southern California Permanent GPS Geodetic Array: Spatial filtering of daily positions for estimating coseismic and postseismic displacements induced by the 1992 Landers earthquake, Journal of Geophysical Research, 102, B8, 18,057-018,070.

Zhang, P., M. Ellis, D. B. Slemmons, and F. Mao (1990), Right-lateral displacements and the Holocene slip rate associated with prehistoric earthquakes along the southern Panamint Valley fault zone: Implications for southern Basin and Range tectonics and coastal California deformation, J. Geophys. Res., 95, 4857 – 4872.

APPENDIX

Table 1: List of stations with location (latitude, longitude), year of installation, east and north velocity components (Ve, Vn), uncertainty in east and north velocities (Se, Sn), Correlation between east and north velocities (CorrNE).

Station	Julian Year	Date	Latitude	Longitude	Ve	Vn	Se	Sn	CorrNE
ALAM	1999.44	99JUN14	37.35	-115.15	0.68	-2.75	0.03	0.07	-0.24
APEX	1999.23	99MAR28	36.31	-114.93	0.91	-2.41	0.05	0.06	-0.27
ARGU	1999.23	99MAR29	36.05	-117.52	6.87	-6.78	0.04	0.08	-0.28
ARMY	2005.72	5-Sep-24	38.49	-118.43	4.95	-5.15	0.1	0.54	0.12
ASHM	2005.69	5-Sep-12	36.34	-116.13	1.57	-2.77	0.06	0.12	0.12
BATM	2005.7	5-Sep-17	36.4	-116.51	2.23	-2.61	0.29	0.13	0.06
BEAT	1999.05	99JAN21	37.04	-116.62	1.48	-3.04	0.08	0.05	-0.24
BEER	2005.59	5-Aug-06	35.55	-117.78	9.63	-7.8	0.55	0.62	0.08
BEPK	2000.68	00SEP07	35.87	-118.07	11.98	-8.54	0.21	0.12	-0.25
BIGP	2005.49	5-Jun-30	37.16	-118.33	7.6	-7.5	0.15	0.24	-0.25
BKAP	2000.95	00DEC14	35.28	-116.08	2.26	-3.25	0.1	0.07	-0.26
BLIN	2005.72	5-Sep-23	37.75	-118.5	5.93	-4.18	0.22	0.2	0.16
BODI	2005.72	5-Sep-24	38.21	-118.96	7.83	-8.46	0.24	0.27	0.09
BONI	2005.69	5-Sep-10	37.22	-117.17	2.11	-3.5	0.09	0.11	0.12
BRID	2005.72	5-Sep-24	38.2	-119.31	8.72	-8.67	0.33	0.15	0.06
BULL	1999.22	99MAR24	36.91	-116.87	1.93	-3.21	0.03	0.05	-0.25
BUST	1999.19	99MAR13	36.74	-116.45	1.43	-2.88	0.02	0.06	-0.27
CCCC	2000.68	00SEP08	35.56	-117.67	11.3	-7.83	0.1	0.09	-0.23
CERR	2005.49	5-Jul-01	36.53	-117.82	5.74	-6.27	0.15	0.19	0.23
CHLO	1999.59	99AUG05	36.74	-116.76	1.85	-3.13	0.03	0.05	-0.25

CHO1	1999.66	99AUG31	39.43	-121.66	7.3	-9.11	0.11	0.13	-0.19
CMBB	1997	97JAN01	38.03	-120.38	8.56	-9.73	0.09	0.12	-0.27
COLU	2005.87	5-Nov-17	38.08	-118.05	4.14	-2.86	0.21	0.25	-0.25
CONW	2005.72	5-Sep-23	38.12	-119.17	8.35	-8.25	0.25	0.38	0.12
COSJ	2005.59	5-Aug-06	36.06	-117.88	7.82	-4.97	0.64	0.79	0.06
COWT	2005.72	5-Sep-23	37.91	-118.79	9.15	-5.78	0.08	0.08	0.13
CPBN	2000.97	00DEC22	35.07	-117.57	13.84	-8.37	0.06	0.08	0.15
CRAM	2005.7	5-Sep-16	37.08	-116.81	1.72	-3.05	0.04	0.08	0.1
CRAT	1999.22	99MAR24	36.8	-116.56	1.55	-2.92	0.03	0.06	-0.25
DECH	2002	2-Jan-04	38.05	-119.09	8.53	-9.14	0.11	0.18	-0.22
DEEP	2005.36	5-May-14	37.34	-118.04	5.43	-5.44	0.08	0.11	0.06
DEVL	2005.69	5-Sep-10	36.43	-116.28	1.55	-2.96	0.1	0.12	0.1
DOBI	2005.72	5-Sep-23	38.05	-118.76	7.98	-6.99	0.2	0.27	0.09
DUNF	2005.69	5-Sep-11	37.31	-117.3	2.35	-3.31	0.14	0.15	0.03
DYER	1999.4	99MAY30	37.74	-118.03	3.49	-4.04	0.03	0.07	-0.23
EAGL	2005.68	5-Sep-09	36.19	-116.36	1.86	-3.43	0.13	0.16	0.16
ECHO	1999.4	99MAY30	37.91	-114.26	0.43	-2.8	0.08	0.08	-0.24
EPAS	2005.85	5-Nov-10	37.92	-117.88	2.9	-2.6	0.26	0.4	0.08
FISH	2005.36	5-May-14	37.56	-118	4.68	-4.29	0.63	0.72	-0.24
FLAT	2005.72	5-Sep-24	38.3	-118.46	4.97	-4.15	0.12	0.15	-0.21
GEMF	2005.36	5-May-15	37.74	-117.29	1.93	-3.63	0.53	0.42	0.08
GOLD	1997	97JAN02	35.42	-116.88	6.92	-4.84	0.09	0.1	-0.25
HELL	2006.57	6-Jul-29	36.72	-116.97	2.47	-3.32	0.16	0.11	0.07
HIGH	2005.68	5-Sep-09	36.28	-116.15	1.49	-2.61	0.08	0.14	0.12
HW95	2005.69	5-Sep-10	37.19	-116.94	2.12	-3.35	0.12	0.16	0.12
IBEX	2006.26	6-Apr-09	35.84	-116.36	2.17	-3.04	0.11	0.18	0.04
ICOR	2005.36	5-May-14	37.46	-117.29	1.06	-4.36	0.12	0.13	0.1
INDE	2005.49	5-Jul-01	36.79	-118.24	9.07	-10.94	0.28	0.47	-0.02

ISLK	1999.76	99OCT07	35.66	-118.47	11.66	-10	0.12	0.11	-0.28
JACK	2005.87	5-Nov-17	38.11	-118.4	5.89	-3.78	0.35	0.13	-0.23
JOHN	1999.26	99APR06	36.45	-116.09	1.29	-2.73	0.05	0.08	-0.24
KENN	2005.59	5-Aug-06	36.03	-118.2	9.05	-8.2	0.38	0.51	-0.22
LAVA	2005.49	5-Jul-01	37.02	-118.18	7.02	-6.25	0.35	0.33	0.27
LAWS	2005.36	5-May-13	37.39	-118.29	7.41	-5.33	0.26	0.25	0.41
LEAD	2005.49	5-Jul-02	36.92	-117.94	4.42	-6.53	0.52	0.45	-0.1
LICE	2006.26	6-Apr-08	36.85	-116.4	1.41	-2.79	0.06	0.1	0.09
LIND	1999.72	99SEP23	36.36	-119.05	9.87	-9.64	0.04	0.05	-0.21
LITT	1999.07	99JAN28	36.74	-116.3	1.31	-2.81	0.05	0.06	-0.26
LNMT	2000.99	00DEC30	35.09	-116.94	9.76	-6.45	0.09	0.1	-0.24
LONP	2005.49	5-Jul-01	36.55	-118.11	8.32	-9.05	0.2	0.25	9.00E-03
LUCK	2005.72	5-Sep-24	38.42	-118.76	5.68	-5.87	0.16	0.17	0.05
MERC	1999.26	99APR07	36.63	-115.97	1.15	-2.68	0.07	0.08	-0.24
MILR	2006.73	6-Sep-27	38.12	-117.44	2.06	-2.63	0.23	0.14	0.05
MINA	2005.87	5-Nov-17	38.42	-118.15	3.18	-3.04	0.24	0.33	0.07
MOHO	2005.87	5-Nov-17	38.24	-118.24	3.77	-2.95	0.14	0.13	0.1
MONT	2005.85	5-Nov-10	38.07	-117.7	2.2	-2.27	0.52	0.31	0.13
MUSB	1997.84	97NOV07	37.17	-119.3	9.21	-9.74	0.11	0.09	-0.25
NEVA	2006.26	6-Apr-08	36.85	-116.31	2.66	-2.35	0.22	0.16	0.02
NOPE	2006.25	6-Apr-04	35.96	-115.98	1.52	-2.74	0.08	0.2	0.08
OASI	2005.69	5-Sep-10	37.03	-116.79	2.07	-3.39	0.09	0.11	-0.26
ORIE	2005.69	5-Sep-11	37.25	-117.45	2.31	-3.7	0.12	0.11	0.1
ORVB	1997	97JAN01	39.55	-121.5	7.06	-9.25	0.08	0.1	-0.19
OWEN	2005.49	5-Jul-01	36.74	-118.05	6.27	-6.71	0.2	0.27	0.34
P056	2005.87	5-Nov-18	36.02	-119.06	10.63	-11.55	0.28	0.15	0.08
P091	2007.12	7-Feb-17	36.61	-117.53	4.49	-4.72	0.68	0.15	0.09
P092	2006.92	6-Dec-06	36.8	-117.4	3.72	-4.02	0.17	0.17	-0.23

P093	2007.24	7-Mar-31	36.6	-117.99	6.88	-6.69	0.2	0.06	0.17
P094	2006.89	6-Nov-23	37.2	-117.7	3.62	-4.38	0.03	0.1	0.09
P462	2006.93	6-Dec-08	36.07	-116.62	2.6	-3.32	0.27	0.25	0.14
P463	2007.3	7-Apr-21	36.02	-117.16	5.42	-4.88	0.18	0.27	0.18
P464	2006.2	6-Mar-16	36.15	-117.41	6.05	-5.66	0.06	0.17	7.00E-03
P465	2007.44	7-Jun-14	36.46	-118.13	10.9	-7.51	0.19	0.32	0.02
P466	2007.36	7-May-13	36.53	-117.78	5.74	-5.86	0.32	0.29	0.07
P467	2006.2	6-Mar-18	36.57	-118.09	7.69	-6.92	0.31	0.35	-0.1
P468	2006.87	6-Nov-17	36.97	-118.11	6.31	-6.59	0.04	0.14	0.08
P469	2007.29	7-Apr-20	37.23	-117.93	4.39	-4.85	0.04	0.15	-0.24
P558	2006.54	6-Jul-20	35.13	-118.61	13.43	-11.8	0.14	0.22	0.05
P566	2005.87	5-Nov-17	36.32	-119.22	9.58	-10.75	0.11	0.09	0.08
P567	2005.55	5-Jul-23	35.42	-118.75	11.21	-11.56	0.09	0.15	0.14
P568	2007.28	7-Apr-16	35.25	-118.12	12.55	-8.82	0.21	0.35	0.08
P569	2007.28	7-Apr-16	35.37	-118.12	11.5	-9.25	0.15	0.28	0.07
P570	2006.58	6-Aug-04	35.66	-118.26	10.97	-9.17	0.04	0.14	0.13
P571	2005.55	5-Jul-23	36.23	-118.76	10.14	-9.05	0.08	0.13	0.16
P572	2006.55	6-Jul-21	36.58	-118.95	9.85	-8.95	0.1	0.11	0.08
P579	2006.45	6-Jun-15	35.03	-118	14.3	-8.75	0.03	0.14	0.08
P580	2007.09	7-Feb-03	35.62	-117.19	8.01	-6.45	0.14	0.25	0.09
P591	2005.48	5-Jun-28	35.15	-118.01	13.65	-8.39	0.09	0.13	0.08
P592	2007.35	7-May-10	35.23	-117.3	10.69	-6.91	0.12	0.25	0.09
P593	2007.08	7-Feb-02	35.38	-117.2	9.43	-6.12	0.1	0.3	0.09
P594	2005.06	5-Jan-23	35.89	-117.39	7.08	-6.55	0.13	0.15	0.02
P595	2005.8	5-Oct-23	35.69	-117.4	8.44	-6.93	0.09	0.09	0.1
P596	2007.12	7-Feb-15	35.99	-116.89	4.45	-4.52	0.21	0.08	0.01
P597	2007.12	7-Feb-17	35.71	-116.88	5.6	-5.94	0.22	0.4	0.07
P611	2006.13	6-Feb-18	35.2	-115.65	1.09	-2.53	0.11	0.24	0.07

P615	2006.38	6-May-21	35.2	-116.76	6.85	-5.27	0.08	0.17	0.08
P616	2007.35	7-May-11	35.42	-117.89	11.33	-8.4	0.12	0.23	0.09
P617	2006.37	6-May-19	35.32	-116.57	4.2	-3.99	0.1	0.11	0.09
P618	2005.99	5-Dec-30	35.14	-116.1	1.47	-3.63	0.05	0.08	6.00E-03
P621	2005.7	5-Sep-15	35.47	-115.54	1.09	-2.56	0.09	0.17	0.1
P622	2005.8	5-Oct-22	35.16	-115.36	1.06	-2.54	0.09	0.15	0.08
P626	2005.82	5-Oct-29	35.29	-115.23	1.09	-2.38	0.13	0.17	-0.25
P627	2006.86	6-Nov-14	37.97	-118.37	5.83	-4.25	0.15	0.19	0.07
P636	2007.45	7-Jun-17	37.96	-119.14	8.93	-9.78	0.06	0.67	0.06
P644	2007.54	7-Jul-20	37.49	-118.68	6.44	-6.77	0.17	0.58	0.08
P649	2006.85	6-Nov-10	37.9	-118.73	8.51	-5.01	0.19	0.22	0.07
P650	2006.82	6-Oct-29	37.89	-118.55	6.84	-4.34	0.04	0.11	0.13
P651	2006.86	6-Nov-11	37.56	-118.38	6.16	-5.29	0.14	0.08	0.13
P652	2007.46	7-Jun-21	37.58	-118.23	5.31	-3.88	0.31	0.62	0.08
P653	2006.81	6-Oct-27	37.73	-118.47	6.47	-4.6	0.19	0.11	0.1
P725	2006.8	6-Oct-21	37.08	-119.74	9.84	-9.37	0.11	0.19	0.13
P726	2006.88	6-Nov-19	37.28	-118.14	5.26	-5.71	0.13	0.22	0.07
P727	2007.45	7-Jun-15	37.27	-118.46	7.57	-7.7	0.36	0.27	0.06
PANA	2005.59	5-Aug-05	36.24	-117.41	4.79	-4.1	0.57	0.9	0
PERL	1999.22	99MAR24	36.9	-116.68	1.67	-3.12	0.05	0.05	-0.23
PHIN	2006.42	6-Jun-04	36.98	-117.03	2.16	-3.01	0.19	0.14	0.03
PILO	2005.87	5-Nov-17	38.27	-117.98	4.01	-3.06	0.38	0.23	0.14
POIN	1999.26	99APR06	36.58	-116.12	1.27	-2.7	0.05	0.07	-0.26
RAIL	1999.4	99MAY30	38.28	-115.66	0.6	-2.93	0.12	0.07	-0.21
RAMT	2000.68	00SEP08	35.33	-117.68	12.05	-7.42	0.09	0.12	-0.24
RELA	1999.22	99MAR24	36.71	-116.55	1.56	-2.91	0.02	0.05	-0.24
REP4	2006.26	6-Apr-06	36.84	-116.46	1.8	-2.58	0.26	0.13	0.1
REPO	1999.22	99MAR24	36.84	-116.46	1.45	-2.99	0.02	0.04	-0.22

RHIL	2006.68	6-Sep-09	38.42	-117.57	1.86	-2.8	0.49	0.64	0.07
ROGE	1999.24	99MAR31	36.21	-117.08	4.07	-4	0.1	0.1	-0.24
ROUG	2005.8	5-Oct-21	38.4	-118.98	6.53	-7.15	0.14	0.29	-0.21
ROYS	2006.73	6-Sep-27	38.26	-117.6	1.7	-3.1	0.12	0.19	-0.24
RUMP	2005.69	5-Sep-11	36.25	-115.86	1.53	-2.84	0.1	0.1	0.11
RYAN	1999.22	99MAR24	36.31	-116.65	2.21	-3.16	0.09	0.06	-0.24
SALI	2005.49	5-Jul-02	36.7	-117.84	5.65	-6.86	0.47	0.36	-0.12
SANA	2006.73	6-Sep-27	38.24	-117.08	2.03	-2.94	0.1	0.2	0.04
SCOT	2005.69	5-Sep-11	37.06	-117.25	2.05	-3.77	0.09	0.11	0.11
SHAK	2005.49	5-Jul-02	37.26	-117.93	4.78	-4.48	0.63	0.88	0.05
SHOS	1999.22	99MAR24	35.97	-116.29	2.6	-2.9	0.08	0.06	-0.29
SKUL	1999.22	99MAR24	36.73	-116.21	1.24	-2.8	0.05	0.09	-0.24
SMYC	1999.22	99MAR24	36.32	-115.58	1.1	-2.57	0.03	0.15	-0.27
STRI	1999.22	99MAR24	36.64	-116.33	1.44	-2.71	0.03	0.06	-0.23
SULF	2005.49	5-Jul-02	37.22	-117.68	3.78	-5.83	0.57	0.61	0.04
SUTB	1997.24	97MAR30	39.2	-121.82	7.03	-9.51	0.13	0.1	-0.18
SYLV	2005.36	5-May-14	37.45	-117.74	3.74	-3.93	0.23	0.19	0.11
TALC	2005.59	5-Aug-05	36.35	-117.71	6.26	-6.05	0.46	0.76	0.05
TATE	1999.22	99MAR24	36.93	-116.57	1.48	-2.9	0.04	0.05	-0.23
THCP	2000.93	00DEC08	35.15	-118.41	13.97	-10.82	0.11	0.09	-0.23
THOM	2005.36	5-May-15	37.94	-117.37	2.5	-3.52	0.3	0.3	0.07
TIVA	1999.22	99MAR24	36.93	-116.23	1.17	-2.72	0.08	0.09	-0.23
TONI	2006.73	6-Sep-27	38.35	-117.29	2.54	-3.21	0.11	0.21	0.12
TONO	1999.22	99MAR24	38.09	-117.18	1.4	-3.04	0.08	0.08	-0.23
UCD1	1997	97JAN01	38.53	-121.75	8.92	-9.57	0.11	0.11	-0.2
UFOS	2005.36	5-May-15	37.39	-117.1	2.19	-3.97	0.1	0.13	0.08
UNR1	2002.77	2-Oct-11	36.24	-115.24	2.03	-2.33	0.12	0.1	-0.25
UNR2	2003.33	3-May-02	36.77	-114.05	2.54	-1.37	0.19	0.19	-0.26

VINE	2006.55	6-Jul-22	36.99	-117.36	2.71	-3.62	0.03	0.2	0.23
VONS	2005.7	5-Sep-16	36.59	-116.62	2.46	-2.67	0.25	0.11	0.05
WATC	2002	2-Jan-04	37.66	-118.65	7.87	-5.34	0.11	0.1	-0.22
WEEP	2005.36	5-May-15	37.85	-117.56	3.32	-3.06	0.23	0.22	-0.24
WOLF	2005.36	5-May-14	37.6	-117.88	3.54	-4.71	0.46	0.57	0.08
ZUMA	2005.36	5-May-14	37.55	-117.49	2.28	-3.15	0.2	0.26	0.09

Table 2: List of angular rotations and uncertainties determined from the model for each block, in radians per year

Blocks	Strain (nanostrains/year)			Uncertainty Strain (nanostrains/year)		
SN	0.0031	0.0073	-0.0167	0.01	0.01	0.01
AA	0.0009	-0.0018	-0.0014	0.01	0.01	0.01
DD	0.0016	0.0026	0.0004	0.01	0.01	0.01
GG	-0.0014	0.0014	-0.0017	0.01	0.01	0.01
HH	-0.0003	0	-0.0018	0.01	0.01	0.01
II	-0.0038	-0.0032	-0.0024	0.01	0.01	0.01
JJ	-0.0006	-0.0004	-0.0003	0.01	0.01	0.01
KK	-0.0003	0.0001	-0.0012	0.01	0.01	0.01
LL	0.0028	0.007	-0.0015	0.01	0.01	0.01
MM	0	-0.0001	-0.0004	0.01	0.01	0.01
NN	-0.0002	0	0	0.01	0.01	0.01
OO	-0.0025	0.0012	-0.0011	0.01	0.01	0.01
PP	-0.0002	0.0002	-0.0004	0.01	0.01	0.01
CB6_7	-0.0012	-0.0002	-0.0013	0.01	0.01	0.01
CB3_4	8.4843	-15.4331	-48.3753	0.8341	0.9803	1.4797
MJ	-19.1657	50.8165	-66.726	0.5757	1.2167	1.2722
QQ	0.0048	0.0002	0.0006	0.01	0.01	0.01
RR	-0.0002	-0.0001	-0.0004	0.01	0.01	0.01
OV	-0.0004	0	-0.001	0.01	0.01	0.01

Table 3: List of strain associated with each block and their uncertainties, calculated from the model, in nanostrains/year. Mojave block, MJ, has been allowed to strain. Rests all were not allowed to deform.

Blocks	Omega (x 10^{-7})			Uncertainty Omega (x 10^{-8})		
SN	-0.021	-0.0095	-0.004	0	0	0
AA	0.0233	0.0798	-0.0749	0.0368	0.068	0.0546
DD	0.0264	0.0614	-0.0538	0.0165	0.0334	0.0265
GG	0.003	0.0285	-0.0322	0.0165	0.0316	0.026
HH	-0.0257	-0.0227	0.0099	0.0318	0.0602	0.0496
II	-0.0046	0.0173	-0.0242	0.012	0.0221	0.0191
JJ	0.0193	0.0516	-0.0512	0.0683	0.1289	0.1098
KK	0.0097	0.0323	-0.0337	0.0435	0.0836	0.0703
LL	0.0007	0.0082	-0.0119	0.0113	0.0222	0.0187
MM	0.0017	0.0082	-0.0117	0.0142	0.0288	0.0241
NN	0.0501	0.1064	-0.0979	0.032	0.061	0.0533
OO	0.0787	0.1631	-0.1482	0.0326	0.0607	0.0534
PP	0.0043	0.0118	-0.015	0.02	0.0427	0.0359
CB6_7	0.0591	0.1317	-0.1126	0.0381	0.0752	0.061
CB3_4	0.1657	0.3546	-0.2875	0.0461	0.0882	0.0694
MJ	**0.0202**	**0.0633**	**-0.0561**	**0.0423**	**0.0834**	**0.0656**
QQ	0.0048	0.0146	-0.016	0.0132	0.0277	0.0224
RR	0.1205	0.2408	-0.2147	0.0608	0.1132	0.0981
OV	0.0269	0.0824	-0.0769	0.0611	0.1153	0.0924

Table 4: List of fault slip rates and their uncertainties along the fault segments in the model.

Fault	Strike Slip	Dip Slip	Extension
1	0.2+/-0.1	2.4+/-0.1	1.7+/-0.1
2	0.4+/-0.1	2.1+/-0.1	1.5+/-0.1
3	0.5+/-0.1	1.9+/-0.1	1.3+/-0.1
4	0.8+/-0.1	1.8+/-0.1	1.3+/-0.1
5	0.4+/-0.1	1.4+/-0.1	1.0+/-0.1
6	0.6+/-0.1	0.5+/-0.1	0.4+/-0.0
7	0.6+/-0.1	-0.3+/-0.1	-0.2+/-0.1
8	0.2+/-0.1	-1.2+/-0.1	-0.8+/-0.1
9	-1.6+/-0.1	0.5+/-0.1	0.4+/-0.1
10	-1.6+/-0.1	0.3+/-0.1	0.2+/-0.1
11	-0.7+/-0.1	-0.6+/-0.1	-0.4+/-0.1
12	-0.6+/-0.1	-1.0+/-0.1	-0.7+/-0.1
13	-0.1+/-0.1	-1.4+/-0.1	-1.0+/-0.1
14	-0.9+/-0.1	-0.7+/-0.1	-0.5+/-0.1
15	-0.9+/-0.1	-0.8+/-0.1	-0.6+/-0.1
16	-0.8+/-0.1	-1.2+/-0.1	-0.8+/-0.1
17	1.3+/-0.1	2.6+/-0.2	0.4+/-0.0
18	3.1+/-0.1	-2.8+/-0.2	-0.5+/-0.0
19	2.9+/-0.1	1.4+/-0.2	0.2+/-0.0

20	3.1+/-0.1	-0.5+/-0.2	-0.1+/-0.0
21	3.2+/-0.1	0.3+/-0.2	0.1+/-0.0
22	3.4+/-0.1	0.1+/-0.2	0.0+/-0.0
23	3.8+/-0.1	-2.0+/-0.2	-0.4+/-0.0
24	3.8+/-0.1	5.2+/-0.2	0.9+/-0.0
25	-2.5+/-0.1	-0.6+/-0.2	-0.1+/-0.0
26	-1.8+/-0.1	5.0+/-0.2	0.9+/-0.0
27	-1.5+/-0.1	1.5+/-0.1	0.3+/-0.0
28	0.0+/-0.1	1.7+/-0.2	0.3+/-0.0
29	1.5+/-0.1	-2.0+/-0.2	-0.4+/-0.0
30	1.4+/-0.1	1.1+/-0.2	0.2+/-0.0
31	-1.5+/-0.1	0.7+/-0.2	0.1+/-0.0
32	0.5+/-0.1	2.4+/-0.1	1.7+/-0.0
33	-1.1+/-0.1	-1.8+/-0.1	-1.3+/-0.1
34	-0.9+/-0.1	-1.8+/-0.1	-1.3+/-0.1
35	-1.4+/-0.1	-1.1+/-0.1	-0.8+/-0.1
36	-1.4+/-0.1	-0.9+/-0.1	-0.6+/-0.1
37	-1.5+/-0.1	-0.5+/-0.1	-0.4+/-0.1
38	-2.3+/-0.1	0.2+/-0.1	0.1+/-0.1
39	-2.2+/-0.1	0.8+/-0.1	0.6+/-0.1
40	0.5+/-0.1	1.6+/-0.1	1.1+/-0.1
41	1.0+/-0.1	-0.1+/-0.1	-0.1+/-0.1

42	0.8+/-0.1	-1.2+/-0.1	-0.9+/-0.1
43	-1.7+/-0.1	-1.5+/-0.1	-1.1+/-0.1
44	-1.1+/-0.1	-2.5+/-0.1	-1.8+/-0.1
45	-1.6+/-0.1	-2.1+/-0.1	-1.5+/-0.1
46	-2.2+/-0.1	-0.8+/-0.1	-0.6+/-0.1
47	-2.0+/-0.1	0.4+/-0.1	0.3+/-0.1
48	-1.9+/-0.1	0.4+/-0.1	0.3+/-0.1
49	-1.9+/-0.1	0.4+/-0.1	0.3+/-0.1
50	-2.0+/-0.1	0.1+/-0.1	0.0+/-0.1
51	-1.7+/-0.1	-0.7+/-0.1	-0.5+/-0.1
52	-1.1+/-0.1	-2.2+/-0.1	-1.6+/-0.1
53	-1.1+/-0.1	-2.5+/-0.1	-1.7+/-0.1
54	1.1+/-0.1	-0.7+/-0.1	-0.5+/-0.1
55	1.1+/-0.1	-0.3+/-0.1	-0.2+/-0.1
56	-0.4+/-0.1	-0.8+/-0.1	-0.5+/-0.1
57	-0.5+/-0.1	-0.1+/-0.1	-0.1+/-0.1
58	-0.5+/-0.1	-0.0+/-0.1	-0.0+/-0.1
59	-0.4+/-0.1	0.8+/-0.1	0.6+/-0.1
60	0.8+/-0.1	-0.4+/-0.1	-0.3+/-0.1
61	0.5+/-0.1	-1.0+/-0.1	-0.7+/-0.1
62	0.2+/-0.1	-1.0+/-0.1	-0.7+/-0.1
63	0.0+/-0.1	-0.8+/-0.1	-0.6+/-0.1

64	0.2+/-0.1	-0.5+/-0.1	-0.4+/-0.1
65	0.1+/-0.1	-0.3+/-0.1	-0.2+/-0.1
66	0.2+/-0.1	0.1+/-0.1	0.1+/-0.1
67	0.2+/-0.1	0.4+/-0.1	0.3+/-0.1
68	-0.7+/-0.0	1.5+/-0.2	0.3+/-0.0
69	-0.7+/-0.0	1.9+/-0.2	0.3+/-0.0
70	-0.7+/-0.0	-1.6+/-0.2	-0.3+/-0.0
71	-0.7+/-0.0	-1.1+/-0.2	-0.2+/-0.0
72	-0.7+/-0.0	0.4+/-0.1	0.1+/-0.0
73	-0.7+/-0.0	2.1+/-0.2	0.4+/-0.0
74	-0.2+/-0.1	-0.6+/-0.1	-0.4+/-0.1
75	-1.4+/-0.0	-1.8+/-0.1	-1.3+/-0.0
76	-1.5+/-0.1	-1.7+/-0.1	-1.2+/-0.0
77	-1.7+/-0.1	-2.0+/-0.1	-1.4+/-0.0
78	-0.2+/-0.1	-0.5+/-0.1	-0.3+/-0.1
79	-0.2+/-0.1	-0.3+/-0.1	-0.2+/-0.1
80	-2.2+/-0.1	-1.4+/-0.1	-1.0+/-0.1
81	-2.3+/-0.1	-1.7+/-0.1	-1.2+/-0.1
82	-2.3+/-0.1	-2.2+/-0.1	-1.6+/-0.1
83	-2.1+/-0.1	-2.8+/-0.1	-2.0+/-0.0
84	-1.3+/-0.1	-4.3+/-0.1	-3.0+/-0.1
85	-1.3+/-0.1	-5.0+/-0.1	-3.5+/-0.1

86	-3.4+/-0.1	-2.6+/-0.1	-1.8+/-0.1
87	-0.5+/-0.0	-3.8+/-0.1	-2.7+/-0.0
88	-0.9+/-0.0	-3.5+/-0.1	-2.5+/-0.0
89	-0.5+/-0.0	-3.5+/-0.1	-2.5+/-0.0
90	-1.8+/-0.0	-2.8+/-0.1	-2.0+/-0.0
91	-0.5+/-0.0	-3.5+/-0.1	-2.4+/-0.0
92	-0.5+/-0.0	-3.3+/-0.1	-2.3+/-0.0
93	-1.5+/-0.0	-2.6+/-0.1	-1.8+/-0.0
94	-2.3+/-0.0	-0.8+/-0.1	-0.5+/-0.0
95	-1.7+/-0.0	-2.1+/-0.1	-1.5+/-0.0
96	-2.3+/-0.0	0.3+/-0.1	0.2+/-0.0
97	-1.7+/-0.0	-2.1+/-0.0	-1.5+/-0.0
98	-1.9+/-0.0	-1.5+/-0.0	-1.0+/-0.0
99	-0.8+/-0.0	-2.8+/-0.0	-2.0+/-0.0
100	-1.2+/-0.0	-2.4+/-0.0	-1.7+/-0.0
101	-1.5+/-0.0	-1.7+/-0.0	-1.2+/-0.0
102	-1.8+/-0.0	-1.0+/-0.0	-0.7+/-0.0
103	-1.9+/-0.0	-0.2+/-0.0	-0.2+/-0.0
104	-1.3+/-0.0	-1.8+/-0.0	-1.3+/-0.0
105	-1.6+/-0.0	-1.1+/-0.0	-0.8+/-0.0
106	-1.3+/-0.0	-1.7+/-0.1	-1.2+/-0.0
107	-1.1+/-0.0	-1.8+/-0.1	-1.3+/-0.0

108	-1.7+/-0.0	-0.6+/-0.1	-0.4+/-0.0
109	-1.5+/-0.0	-1.2+/-0.1	-0.8+/-0.0
110	-1.4+/-0.0	-1.2+/-0.1	-0.9+/-0.0
111	-1.7+/-0.0	-0.2+/-0.1	-0.1+/-0.0
112	-1.7+/-0.0	-0.4+/-0.1	-0.2+/-0.0
113	-1.6+/-0.0	0.0+/-0.1	0.0+/-0.0
114	-0.1+/-0.1	-0.2+/-0.1	-0.2+/-0.1
115	0.0+/-0.1	-0.5+/-0.1	-0.3+/-0.1
116	0.0+/-0.1	-0.7+/-0.1	-0.5+/-0.1
117	-0.2+/-0.1	-0.7+/-0.1	-0.5+/-0.1
118	-0.3+/-0.1	-0.9+/-0.1	-0.6+/-0.1
119	-0.5+/-0.1	-0.9+/-0.1	-0.6+/-0.1
120	-1.1+/-0.1	-0.7+/-0.1	-0.5+/-0.1
121	-1.0+/-0.1	-0.4+/-0.1	-0.3+/-0.1
122	-1.0+/-0.1	0.2+/-0.1	0.2+/-0.0
123	-1.2+/-0.1	0.6+/-0.1	0.5+/-0.1
124	-1.2+/-0.1	0.8+/-0.1	0.6+/-0.1
125	-1.0+/-0.1	0.9+/-0.1	0.7+/-0.1
126	-0.6+/-0.1	1.8+/-0.1	1.3+/-0.1
127	0.6+/-0.1	-2.3+/-0.1	-1.7+/-0.0
128	-0.0+/-0.0	-0.4+/-0.1	-0.3+/-0.0
129	0.0+/-0.0	-0.4+/-0.1	-0.3+/-0.0

130	0.3+/-0.0	0.0+/-0.1	0.0+/-0.0
131	0.2+/-0.0	-0.2+/-0.1	-0.2+/-0.0
132	0.1+/-0.0	-0.3+/-0.1	-0.2+/-0.0
133	0.1+/-0.0	-0.3+/-0.1	-0.2+/-0.0
134	0.1+/-0.0	-0.3+/-0.1	-0.2+/-0.0
135	0.0+/-0.0	-0.3+/-0.1	-0.2+/-0.0
136	-0.0+/-0.0	-0.3+/-0.1	-0.2+/-0.0
137	0.0+/-0.0	-0.2+/-0.1	-0.2+/-0.1
138	0.1+/-0.0	-0.2+/-0.1	-0.2+/-0.1
139	0.1+/-0.0	-0.2+/-0.1	-0.1+/-0.1
140	-0.0+/-0.1	-0.2+/-0.1	-0.1+/-0.1
141	-0.3+/-0.1	-0.5+/-0.1	-0.3+/-0.0
142	-0.5+/-0.1	-0.3+/-0.1	-0.2+/-0.1
143	-0.1+/-0.1	-0.7+/-0.1	-0.5+/-0.1
144	0.4+/-0.1	-0.6+/-0.1	-0.4+/-0.1
145	1.3+/-0.1	-0.2+/-0.1	-0.2+/-0.0
146	1.1+/-0.0	1.0+/-0.1	0.7+/-0.0
147	-0.1+/-0.1	-0.7+/-0.1	-0.5+/-0.1
148	-0.3+/-0.1	-0.5+/-0.1	-0.3+/-0.0
149	-0.2+/-0.1	-0.5+/-0.1	-0.4+/-0.0
150	-0.3+/-0.1	-0.4+/-0.1	-0.3+/-0.0
151	-0.1+/-0.1	-0.5+/-0.1	-0.4+/-0.1

152	-0.2+/-0.1	-0.4+/-0.1	-0.3+/-0.0
153	-0.2+/-0.1	-0.2+/-0.1	-0.2+/-0.1
154	-0.2+/-0.1	-0.1+/-0.1	-0.1+/-0.1
155	-0.2+/-0.1	-0.3+/-0.1	-0.2+/-0.1
156	-0.2+/-0.1	-0.2+/-0.1	-0.1+/-0.1
157	-0.2+/-0.1	-0.1+/-0.1	-0.1+/-0.1
158	-0.1+/-0.1	0.3+/-0.1	0.2+/-0.1
159	-0.2+/-0.1	0.0+/-0.1	0.0+/-0.1
160	-0.2+/-0.1	-0.1+/-0.1	-0.1+/-0.1
161	-0.2+/-0.1	-0.2+/-0.1	-0.1+/-0.1
162	-0.2+/-0.1	-0.4+/-0.1	-0.3+/-0.1
163	-0.1+/-0.1	-0.7+/-0.1	-0.5+/-0.1
164	-0.2+/-0.1	-0.9+/-0.1	-0.7+/-0.1
165	-0.2+/-0.1	-0.4+/-0.1	-0.3+/-0.1
166	-0.2+/-0.1	-0.4+/-0.1	-0.3+/-0.1
167	-0.3+/-0.1	-0.2+/-0.1	-0.1+/-0.1
168	-0.9+/-0.1	-1.2+/-0.2	-0.2+/-0.0
169	-0.9+/-0.0	-0.2+/-0.1	-0.1+/-0.0
170	-1.0+/-0.1	1.0+/-0.1	0.2+/-0.0
171	-0.5+/-0.1	1.3+/-0.2	0.2+/-0.0
172	-0.3+/-0.1	-0.8+/-0.2	-0.1+/-0.0
173	-0.2+/-0.1	-0.0+/-0.2	-0.0+/-0.0

174	-0.3+/-0.0	-0.1+/-0.1	-0.0+/-0.0
175	-0.3+/-0.0	-0.3+/-0.1	-0.1+/-0.0
176	-0.4+/-0.0	-0.1+/-0.1	-0.0+/-0.0
177	-0.4+/-0.0	0.3+/-0.1	0.1+/-0.0
178	-0.5+/-0.0	0.4+/-0.1	0.1+/-0.0
179	-1.0+/-0.1	-0.7+/-0.2	-0.1+/-0.0
180	-0.2+/-0.0	1.8+/-0.2	0.3+/-0.0
181	-0.4+/-0.0	-0.3+/-0.1	-0.0+/-0.0
182	-1.5+/-0.1	1.1+/-0.3	0.2+/-0.0
183	1.5+/-0.1	1.3+/-0.1	0.9+/-0.1
184	1.3+/-0.1	1.3+/-0.1	0.9+/-0.1
185	0.7+/-0.1	1.8+/-0.1	1.3+/-0.1
186	0.2+/-0.1	1.9+/-0.1	1.4+/-0.1
187	-1.1+/-0.1	0.5+/-0.1	0.4+/-0.1
188	-0.7+/-0.0	-0.2+/-0.1	-0.2+/-0.0
189	-0.8+/-0.1	1.4+/-0.2	0.3+/-0.0
190	-1.4+/-0.1	-0.9+/-0.2	-0.2+/-0.0